

# Optical Tests of Foundations of Quantum Theory

*Yanhua H. Shih*

- 16.1 Introduction – 386**
  - 16.1.1 Locality – 386
  - 16.1.2 Reality – 387
  - 16.1.3 Complementarity – 389
- 16.2 EPR-Bohm-Bell Correlation and Bell’s Inequality – 390**
  - 16.2.1 Biphoton and Bell State Preparation – 392
  - 16.2.2 Bell State Simulation of Thermal Light – 400
  - 16.2.3 Bell’s Inequality – 406
- 16.3 Scully’s Quantum Eraser – 411**
  - 16.3.1 Random Delayed Choice Quantum Eraser One – 412
  - 16.3.2 Random Delayed Choice Quantum Eraser Two – 416
- 16.4 Popper’s Experiment – 421**
  - 16.4.1 Popper’s Experiment One – 422
  - 16.4.2 Popper’s Experiment Two – 427
- 16.5 Conclusion – 433**
  - References – 433**

Y.H. Shih (✉)  
Department of Physics, University of Maryland, Baltimore, MD 21250, USA  
e-mail: [shih@umbc.edu](mailto:shih@umbc.edu)

## 16.1 Introduction

Since the beginning of Quantum Theory scientists questioned its very basic concepts, such as locality, reality, and complementarity, because they are so different from classical theory and from our everyday experience.

### 16.1.1 Locality

Einstein posed his students a question [1]: suppose a photon with energy  $h\nu$  is created from a point source, such as an atomic transition; how big is the photon after propagating 1 year? This question seems easy to answer. Since the photon is created from a point source, it would propagate in the form of a spherical wave and its wavefront must be a sphere with a diameter of 2 lightyears after 1 year propagating. Einstein then asked again: suppose a point-like photon counting detector located on the surface of the big sphere is triggered by that photon, how long does it take for the energy on the other side of the big sphere to arrive at the detector? Two years? For a fast photodetector, it takes only a few picoseconds to produce a photoelectron by annihilating a photon with energy  $h\nu$ . Does this mean something has happened faster than the speed of light? Bohr provided a famous answer to this question: the “wavefunction collapses” instantaneously! Why does the wavefunction need to “collapse”? Bohr did not explain. In quantum theory, perhaps, the wavefunction does not need to “collapse.” A wavefunction is defined as the probability amplitude for a particle to be observed at a space-time coordinate  $(\mathbf{r}, t)$ .

Quantum theory, however, does allow nonlocal interference. Assuming Einstein continued his question: if two photons are created simultaneously from the point source, and we set up a measurement with two different yet indistinguishable alternative ways for the photon pair to produce a joint photodetection event between two distant point-like photon counting detectors, what is the chance to observe a joint photodetection event at  $(\mathbf{r}_1, t_1)$  and  $(\mathbf{r}_2, t_2)$ ? According to quantum theory, the probability is the result of the linear superposition between the two probability amplitudes,

$$P(\mathbf{r}_1, t_1; \mathbf{r}_2, t_2) = |\mathcal{A}_I(\mathbf{r}_1, t_1; \mathbf{r}_2, t_2) + \mathcal{A}_{II}(\mathbf{r}_1, t_1; \mathbf{r}_2, t_2)|^2 \quad (16.1)$$

despite the distance between the two photodetection events, even if the two detectors are placed on the opposite sides of the big sphere.<sup>1</sup> How much time for this superposition to complete? Two years? Again, the two-photon interference must be completed within the “coincidence” time window which can be a few picoseconds. Furthermore, it is not necessary to use a hardware coincidence counter to count the coincidences. Two independent “event timers,” which record the registration times of the two photodetection events of the two photon counting detectors, respectively, and PC software are able to calculate the joint photodetection probability. In some experiments, one detector-event timer package is placed on a satellite and the other one is placed in a ground laboratory. The recorded history of photodetection events are later brought together at the ground laboratory and analyzed by a PC. We found that the two-photon interferences are observable only when the time axis of the two event timers is correctly synchronized within the response time of the photodetectors which could be a few picoseconds.

<sup>1</sup> This kind superposition has been named two-photon interference: a pair of photon interferes with the pair itself at distance.

### 16.1.2 Reality

Now, we ask a different kind of question: Does Einstein's photon have a defined momentum and position over the course of its propagation? On one hand, the photodetection event of a point-like photon counting detector tells us that the annihilated photon at  $(\mathbf{r}, t)$  must carry momentum  $\mathbf{p} = (\hbar\omega/c)\hat{\mathbf{n}}$ , where  $\hat{\mathbf{n}}$  is the unit vector normal to the sphere; on the other hand, Einstein's spherical wavefunction means the momentum of that photon cannot be a constant vector when it is created at the point source of  $(\mathbf{r}_0, t_0)$ , otherwise it would not propagate to all  $4\pi$  directions, yet, the uncertainty principle prevents a point source from producing a photon with  $\Delta\mathbf{p} = 0$ . Does it mean the photon has no momentum in the course of its propagation until its annihilation? To Einstein, the statement from Copenhagen "no phenomenon is a phenomenon until it is a registered phenomenon" [1] was unacceptable! Einstein believed a photon must be created and propagated with a defined momentum, the same as that observed from its annihilation. In Einstein's opinion, momentum and position must be physical realities accompany with a photon, otherwise, we may have to accept that some kinds of phenomena happen faster than the speed of light, such as "wavefunction collapse," or we may have to accept that a photon can be divided into parts, or that part of  $h\nu$  is able to excite a photoelectron.

In 1935, Einstein, Podolsky, and Rosen (EPR) published an article to defend their opinion on physical reality [2]. In that article, EPR proposed a *gedankenexperiment* and introduced an entangled two-particle system based on the superposition of two-particle wavefunctions. The EPR system is composed of two distant interaction-free particles which are characterized by the following wavefunction:

$$\begin{aligned}\Psi(x_1, x_2) &= \frac{1}{2\pi\hbar} \int dp_1 dp_2 \delta(p_1 + p_2) e^{ip_1(x_1 - x_0)/\hbar} e^{ip_2 x_2/\hbar} \\ &= \delta(x_1 - x_2 - x_0)\end{aligned}\quad (16.2)$$

where  $e^{ip_1(x_1 - x_0)/\hbar}$  and  $e^{ip_2 x_2/\hbar}$  are the eigenfunctions, with eigenvalues  $p_1 = p$  and  $p_2 = -p$ , respectively, of the momentum operators  $\hat{p}_1$  and  $\hat{p}_2$  associated with particles 1 and 2;  $x_1$  and  $x_2$  are the coordinate variables to describe the positions of particles 1 and 2, respectively; and  $x_0$  is a constant. The EPR state is very peculiar. Although there is no interaction between the two distant particles, the two-particle superposition cannot be factorized into a product of two individual superpositions of two particles. Quantum theory does not prevent such states.

What can we learn from the EPR state of Eq. (16.2)?

- (1) In the coordinate representation, the wavefunction is a delta function:  $\delta(x_1 - x_2 - x_0)$ . The two particles are always separated in space with a constant value of  $x_1 - x_2 = x_0$ , although the coordinates  $x_1$  and  $x_2$  of the two particles are both unspecified.
- (2) The delta wavefunction  $\delta(x_1 - x_2 - x_0)$  is the result of the superposition of the plane wavefunctions of free particle one,  $e^{ip_1(x_1 - x_0)/\hbar}$ , and free particle two,  $e^{ip_2 x_2/\hbar}$ , with a particular distribution  $\delta(p_1 + p_2)$ . It is  $\delta(p_1 + p_2)$  that made the superposition special: although the momentum of particle one and particle two may take on any values, the delta function restricts the superposition with only these terms in which the total momentum of the system takes a constant value of zero.

Now, we transfer the wavefunction from coordinate representation to momentum representation:

$$\begin{aligned}\Psi(p_1, p_2) &= \frac{1}{2\pi\hbar} \int dx_1 dx_2 \delta(x_1 - x_2 - x_0) e^{-ip_1(x_1 - x_0)/\hbar} e^{-ip_2 x_2/\hbar} \\ &= \delta(p_1 + p_2).\end{aligned}\quad (16.3)$$

What can we learn from the EPR state of Eq. (16.3)?

- (1) In the momentum representation, the wavefunction is a delta function:  $\delta(p_1 + p_2)$ . The total momentum of the two-particle system takes a constant value of  $p_1 + p_2 = 0$ , although the momenta  $p_1$  and  $p_2$  are both unspecified.
- (2) The delta wavefunction  $\delta(p_1 + p_2)$  is the result of the superposition of the plane wavefunctions of free particle one,  $e^{-ip_1(x_1 - x_0)/\hbar}$ , and free particle two,  $e^{-ip_2 x_2/\hbar}$ , with a particular distribution  $\delta(x_1 - x_2 - x_0)$ . It is  $\delta(x_1 - x_2 - x_0)$  that made the superposition special: although the coordinates of particle one and particle two may take on any values, the delta function restricts the superposition with only these terms in which  $x_1 - x_2$  is a constant value of  $x_0$ .

In an EPR system, *the value of the momentum (position) is not determined for either single subsystem. However, if one of the subsystems is measured to be at a certain momentum (position), the other one is determined to have a unique corresponding value despite the distance between them.* An idealized EPR state of a two-particle system is therefore characterized by  $\Delta(p_1 + p_2) = 0$  and  $\Delta(x_1 - x_2) = 0$  simultaneously, even if the momentum and position of each individual free particle are completely undefined, i.e.,  $\Delta p_j \sim \infty$  and  $\Delta x_j \sim \infty$ ,  $j = 1, 2$ . In other words, each of the subsystems may have completely random values or all possible values of momentum and position in the course of their motion, but the correlations of the two subsystems are determined with certainty whenever a joint measurement is performed.<sup>2</sup>

According to EPR's criteria:

**Locality** - There is no action-at-a-distance;

**Reality** - If, without in any way disturbing a system, we can predict with certainty the value of a physical quantity, then there exists an element of physical reality corresponding to this quantity;

**Completeness** - Every element of the physical reality must have a counterpart in the complete theory;

momentum and position must be physical realities associated with particle one and two. This led to the title of their 1935 article: "Can Quantum-Mechanical Description of Physical Reality Be Considered Complete?" [2]

In early 1950s, Bohm simplified EPR's entangled two-particle state of continuous space-time variables to discrete spin variables [3]. Bohm suggested the singlet state of two spin 1/2 particles:

$$|\Psi\rangle = \frac{1}{\sqrt{2}} [|\uparrow\rangle_1 |\downarrow\rangle_2 - |\downarrow\rangle_1 |\uparrow\rangle_2] \quad (16.4)$$

2 There have been arguments considering  $\Delta(p_1 + p_2)\Delta(x_1 - x_2) = 0$  a violation of the uncertainty principle. This argument is false. It is easy to find that  $p_1 + p_2$  and  $x_1 - x_2$  are not conjugate variables. As we know, non-conjugate variables correspond to commuting operators in quantum mechanics, if the corresponding operators exist. To have  $\Delta(p_1 + p_2) = 0$  and  $\Delta(x_1 - x_2) = 0$  simultaneously, or to have  $\Delta(p_1 + p_2)\Delta(x_1 - x_2) = 0$  is not a violation of the uncertainty principle.

where the kets  $|\uparrow\rangle$  and  $|\downarrow\rangle$  represent the states of spin “up” and spin “down,” respectively, along an *arbitrary* direction. Again, for this state, *the spin of neither particle is determined; however, if one particle is measured to be spin up along a certain direction, the other one must be spin down along that direction, despite the distance between the two spin 1/2 particles.* Similar to the original EPR state, Eq. (16.4) is independent of the choice of the spin directions and the eigenstates of the associated non-commuting spin operators.

The most widely used entangled two-particle states might have been the “Bell states” (or EPR-Bohm-Bell states) [4]. Bell states are a set of polarization states for a pair of entangled photons. The four Bell states which form a complete orthonormal basis of two-photon states are usually represented as

$$\begin{aligned} |\Phi_{12}^{(\pm)}\rangle &= \frac{1}{\sqrt{2}} [ |0_1 0_2\rangle \pm |1_1 1_2\rangle ], \\ |\Psi_{12}^{(\pm)}\rangle &= \frac{1}{\sqrt{2}} [ |0_1 1_2\rangle \pm |1_1 0_2\rangle ] \end{aligned} \quad (16.5)$$

where  $|0\rangle$  and  $|1\rangle$  represent two arbitrary orthogonal polarization bases, for example,  $|0\rangle = |H\rangle$  (horizontal linear polarization) and  $|1\rangle = |V\rangle$  (vertical linear polarization); or  $|0\rangle = |R\rangle$  (right-hand circular polarization) and  $|1\rangle = |L\rangle$  (left-hand circular polarization). We will have a detailed discussion of Bell states based on two types of experiments: (1) EPR-Bohm-Bell correlation measurement; and (2) Bell’s inequality testing.

### 16.1.3 Complementarity

Wave-particle duality, which Feynman called the basic mystery of quantum mechanics [5], says that there is always a trade-off between the knowledge of the particle-like and wave-like behavior of a quantum system. In slightly different words, Bohr suggested a complementarity principle in 1927: one can never measure the precise position and momentum of a quantum simultaneously [6]. Since then, complementarity has often been superficially identified with the “wave-particle duality of matter.” How quantum mechanics enforces complementarity may vary from one experimental situation to another (■ Fig. 16.1).

In a single-photon Young’s double-slit experiment, is the photon going to pass “both slits” like a wave or will it choose “which slit” to pass like a particle? This question has been asked since the early days of quantum mechanics [8]. Among most physicists, the common “understanding” is that the position-momentum uncertainty relation makes it impossible to determine which slit a photon or wavepacket passes through without at the same time disturbing the photon or wavepacket enough to destroy the interference pattern. However, it has been shown that under certain circumstances this common “understanding” may not be true. In 1982, Scully and Drühl showed that a “quantum eraser” may erase the which-path information [9]. The “random delayed choice quantum eraser” has been experimentally demonstrated with interesting results: the which-path information is truly erasable even after the annihilation of the quantum itself [10, 11].

Popper’s thought experiment evaluated the same fundamental problem from a slightly different position [12]. Popper proposed a coincidence measurement on a pair of entangled particles. If the position of particle one is learned within  $\Delta y$  through the joint measurement of its twin, particle two, do we expect an uncertainty relation on particle one  $\Delta y \Delta p_y \geq \hbar$ ? Namely, if we place an array of detectors at a distance at which particle one is restricted within  $\Delta y$ , do we expect a diffraction pattern with a minimum width that is determined by  $\Delta y \Delta p_y \geq \hbar$ ?



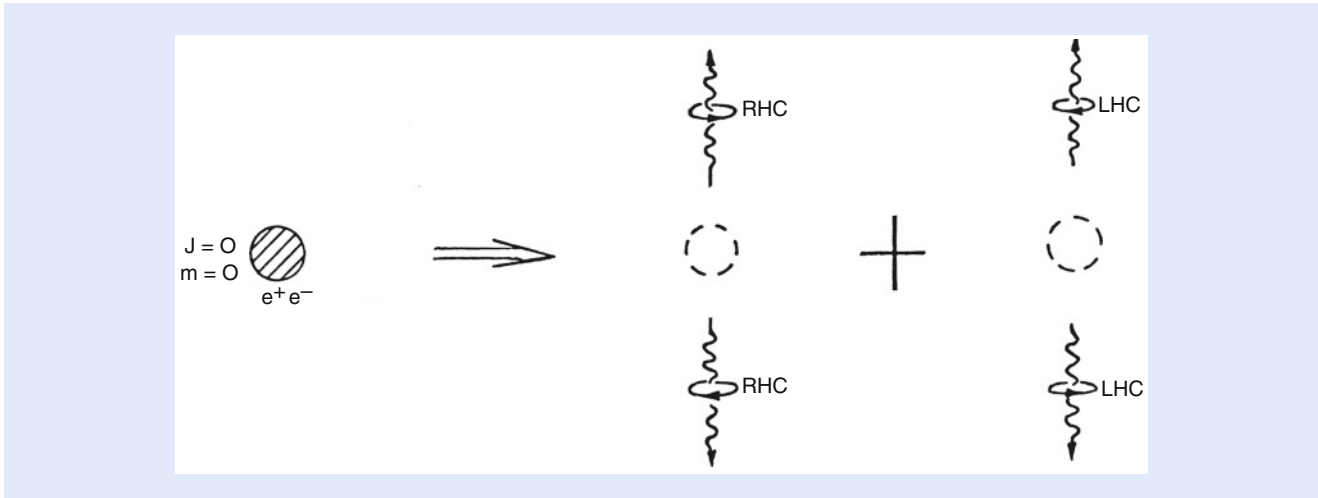
■ **Fig. 16.1** On one hand, a photon can never be divided into parts; on the other hand, we never lose interference at the single photon level. In fact, according to quantum theory, Young's double-slit interference is a single-photon phenomenon. In Diracs terms: "... photon ... only interferes with itself" [7]

Popper predicted a negative answer: particle one would not be diffracted unless a real slit of  $\Delta y$  is inserted. Similar to Einstein, Popper was a believer of realism. In his opinion, a particle must have defined momentum and position over the course of its propagation. We will review two experimental realizations of Popper's thought experiment. It is interesting to see that both experiments, one based on the measurement of entangled photon pairs, another based on the measurement of randomly paired photons in a thermal state, produced a similar result that  $\Delta y \Delta p_y < \hbar$ , agreeing with Popper's prediction [13, 14]. Is this result a violation of the uncertainty principle?

In the following, we will focus on three types of "optical tests of foundations of quantum theory": (1) EPR-Bohm-Bell correlation and Bell's inequality; (2) Quantum eraser; (3) Popper's experiment.

## 16.2 EPR-Bohm-Bell Correlation and Bell's Inequality

An important step to perform an optical test of the EPR-Bohm-Bell correlation and Bell's inequality is to prepare an entangled photon pairs in Bell state. Historically, the most popular entangled photon sources have been: (1) annihilation of positronium; (2) atomic cascade decay; (3) spontaneous parametric down-conversion (SPDC). Both atomic cascade decay and SPDC have been experimentally tested. Most of the early EPR-Bohm-Bell experiments demonstrated in the 1970s and early 1980s used atomic cascade decay [15–20]. Since Alley and Shih introduced SPDC to the preparation of entangled states in the middle of 1980s [21], the signal-idler photon pair of SPDC has played an important role, especially in the tests of Bell's inequality. Using SPDC now-a-days one could easily observe a violation of Bell's inequality with hundreds of standard deviations [22]. The photon pair produced from SPDC has received an interesting name: *biphoton* [23].



■ **Fig. 16.2** Annihilation of Positronium. Due to the conservation of angular momentum, if photon 1 is right-hand circular (RHC) polarized, photon 2 must be right-hand circular polarized. If photon 1 is left-hand circular (LHC) polarized, then photon 2 has to be left-hand circular polarized

■ **Figure 16.2** schematically illustrates the pair-creation mechanism of positronium annihilation [5]. Initially, we have a positron and an electron in the spin-zero state with antiparallel spins. The positronium cannot exist very long: it disintegrates into two  $\gamma$ -ray photons within  $\sim 10^{-10}$  s of its lifetime. The spin zero state is symmetric under all rotations. Therefore, the photon pair may disintegrate into any direction in space with equal probability. The conservation of linear momentum, however, guarantees that if one of the photons is observed in a certain direction, its twin must be found in the opposite direction (with finite uncertainty  $\Delta(\mathbf{p}_1 + \mathbf{p}_2) \neq 0$ ). The conservation of angular momentum will decide the polarization state of the photon pair. As shown in ■ **Fig. 16.2**, in order to keep spin-zero, if photon 1 is right-hand circular polarized (RHC), photon 2 must also be right-hand circular polarized. The same argument shows that if photon 1 is left-hand circular (LHC) polarized, then photon 2 has to be left-hand circular polarized too. Therefore, the positronium may decay into two RHC photons or two LHC photons with equal probability.

Furthermore, the law of parity conservation must be satisfied in the disintegration: the spin-zero ground state of positronium holds an odd parity. Thus, the state of the photon pair must keep its parity odd:

$$|\Psi\rangle = \frac{1}{\sqrt{2}}[|R_1\rangle|R_2\rangle - |L_1\rangle|L_2\rangle], \quad (16.6)$$

which is a non-factorizable pure state of a special superposition between the RHC and LHC states specified with a relative phase of  $\pi$ . Mathematically, “non-factorizable” means that the state cannot be written as a product state of photon 1 and photon 2. Physically, it means that photon 1 and photon 2 are not independent despite the distance between them. The two  $\gamma$ -ray photons are in an entangled polarization state, or spin state. The high energy  $\gamma$ -ray photon pair disintegrated from the annihilation of positronium is a good example to explore the physics of the EPR-Bohm state, however, the  $\gamma$ -ray photon pairs are difficult to handle experimentally: (1) There are no effective polarization analyzers available for the high energy  $\gamma$ -rays; (2) The uncertainty in momentum correlation,  $\Delta(\mathbf{p}_1 + \mathbf{p}_2)$ , has considerable large value, resulting in a “pair collection efficiency loophole” in Bell’s inequality measurements, i.e., one may never have  $\sim 100\%$  chance to “collect” a pair for joint photo-detection measurement [15]. Fortunately, the two-photon state of Eq. (16.6) is also observed in atomic cascade decay with

visible-ultraviolet wavelengths and we have plenty of high efficiency polarization analyzers available in that wavelengths. Thus, most of the early EPR-Bohm-Bell experiments demonstrated in the 1970s and early 1980s used two-photon source of atomic cascade decay [15]. These experiments, unfortunately, still experienced the difficulties in the momentum uncertainty. The “pair collection” efficiency is as low as that of the annihilation of positronium. It was in the middle of 1980s, Alley and Shih introduced the nonlinear optical spontaneous parametric down-conversion to the preparation of entangled states [21]. The entangled signal-idler photon pair can be easily prepared in visible-infrared wavelengths, and very importantly, the uncertainty in momentum correlation was improved significantly. The “pair collection efficiency loophole” was finally removed.

### 16.2.1 Biphoton and Bell State Preparation

The state of a signal-idler photon pair created in SPDC is a typical EPR state [24]. Roughly speaking, the process of SPDC involves sending a pump laser beam into a nonlinear material, such as a non-centrosymmetric crystal. Occasionally, the nonlinear interaction leads to the annihilation of a high frequency pump photon and the simultaneous creation of a pair of lower frequency signal-idler photons into an entangled two-photon state:

$$|\Psi\rangle = \Psi_0 \sum_{s,i} \delta(\omega_s + \omega_i - \omega_p) \delta(\mathbf{k}_s + \mathbf{k}_i - \mathbf{k}_p) a_s^\dagger(\mathbf{k}_s) a_i^\dagger(\mathbf{k}_i) |0\rangle \quad (16.7)$$

where  $\omega_j, \mathbf{k}_j (j = s, i, p)$  are the frequency and wavevector of the signal (s), idler (i), and pump (p),  $a_s^\dagger$  and  $a_i^\dagger$  are creation operators for the signal and the idler photon, respectively, and  $\Psi_0$  is the normalization constant. We have assumed a CW monochromatic laser pump, i.e.,  $\omega_p$  and  $\mathbf{k}_p$  are considered as constants. The two delta functions in Eq. (16.7) are technically named as phase matching condition:

$$\omega_p = \omega_s + \omega_i, \quad \mathbf{k}_p = \mathbf{k}_s + \mathbf{k}_i. \quad (16.8)$$

The names *signal* and *idler* are historical leftovers. The names probably came about due to the fact that in the early days of SPDC, most of the experiments were done with non-degenerate processes. One radiation was in the visible range (and thus easily detected, the signal), and the other was in IR range (usually not detected, the idler). We will see in the following discussions that the role of the idler is not any less than that of the signal. The SPDC process is referred to as type-I if the signal and idler photons have identical polarizations, and type-II if they have orthogonal polarizations. The process is said to be *degenerate* if the SPDC photon pair have the same free space wavelength (e.g.,  $\lambda_i = \lambda_s = 2\lambda_p$ ), and *nondegenerate* otherwise. In general, the pair exit the crystal *non-collinearly*, that is, propagate to different directions defined by the second equation in Eq. (16.8) and the Snell’s law. Of course, the pair may also exit *collinearly*, in the same direction, together with the pump.

The state of the signal-idler pair can be derived, quantum mechanically, by the first order perturbation theory with the help of the nonlinear interaction Hamiltonian. The SPDC interaction arises in a nonlinear crystal driven by a pump laser beam. The polarization, i.e., the dipole moment per unit volume, is given by

$$P_i = \chi_{i,j}^{(1)} E_j + \chi_{i,j,k}^{(2)} E_j E_k + \chi_{i,j,k,l}^{(3)} E_j E_k E_l + \dots \quad (16.9)$$



where  $\chi^{(m)}$  is the  $m$ th order electrical susceptibility tensor. In SPDC, it is the second order nonlinear susceptibility  $\chi^{(2)}$  that plays the role. The second order nonlinear interaction Hamiltonian can be written as

$$H = \varepsilon_0 \int_V d\mathbf{r} \chi_{ijk}^{(2)} E_i E_j E_k \quad (16.10)$$

where the integral is taken over the interaction volume  $V$ .

It is convenient to use the Fourier representation for the electrical fields in Eq. (16.10):

$$\mathbf{E}(\mathbf{r}, t) = \int d\mathbf{k} [\mathbf{E}^{(-)}(\mathbf{k}) e^{-i(\omega(\mathbf{k})t - \mathbf{k} \cdot \mathbf{r})} + \mathbf{E}^{(+)}(\mathbf{k}) e^{i(\omega(\mathbf{k})t - \mathbf{k} \cdot \mathbf{r})}]. \quad (16.11)$$

Substituting Eq. (16.11) into Eq. (16.10) and keeping only the terms of interest, we obtain the SPDC Hamiltonian in the interaction representation:

$$H_{\text{int}}(t) = \varepsilon_0 \int_V d\mathbf{r} \int d\mathbf{k}_s d\mathbf{k}_i \chi_{lmn}^{(2)} E_p^{(+)} E_l^{(+)} e^{i(\omega_p t - \mathbf{k}_p \cdot \mathbf{r})} E_s^{(-)} e^{-i(\omega_s(\mathbf{k}_s)t - \mathbf{k}_s \cdot \mathbf{r})} E_i^{(-)} e^{-i(\omega_i(\mathbf{k}_i)t - \mathbf{k}_i \cdot \mathbf{r})} + h.c., \quad (16.12)$$

where  $h.c.$  stands for Hermitian conjugate. To simplify the calculation, we have also assumed the pump field to be plane and monochromatic with wave vector  $\mathbf{k}_p$  and frequency  $\omega_p$ .

It is easily noticeable that in Eq. (16.12), the volume integration can be done for some simplified cases. At this point, we assume that  $V$  is infinitely large. Later, we will see that the finite size of  $V$  in longitudinal and/or transversal directions may have to be taken into account. For an infinite volume  $V$ , the interaction Hamiltonian Eq. (16.12) is written as

$$H_{\text{int}}(t) = \varepsilon_0 \int d\mathbf{k}_s d\mathbf{k}_i \chi_{lmn}^{(2)} E_p^{(+)} E_s^{(-)} E_i^{(-)} \times \delta(\mathbf{k}_p - \mathbf{k}_s - \mathbf{k}_i) e^{i(\omega_p - \omega_s(\mathbf{k}_s) - \omega_i(\mathbf{k}_i))t} + h.c. \quad (16.13)$$

It is reasonable to consider the pump field classical, which is usually a laser beam, and quantize the signal and idler fields, which are both in single-photon level:

$$E^{(-)}(\mathbf{k}) = i\sqrt{\frac{2\pi\hbar\omega}{V}} a^\dagger(\mathbf{k}), \quad (16.14)$$

$$E^{(+)}(\mathbf{k}) = i\sqrt{\frac{2\pi\hbar\omega}{V}} a(\mathbf{k}),$$

where  $a^\dagger(\mathbf{k})$  and  $a(\mathbf{k})$  are photon creation and annihilation operators, respectively. The state of the emitted photon pair can be calculated by applying the first order perturbation

$$|\Psi\rangle = -\frac{i}{\hbar} \int dt H_{\text{int}}(t) |0\rangle. \quad (16.15)$$

By using vacuum  $|0\rangle$  for the initial state in Eq. (16.15), we assume that there is no input radiation in any signal and idler modes, that is, we have a spontaneous parametric down conversion (SPDC) process.

Further assuming an infinite interaction time, evaluating the time integral in Eq. (16.15) and omitting altogether the constants and slow (square root) functions of  $\omega$ , we obtain the *entangled* two-photon state of Eq. (16.7) in the form of integral:

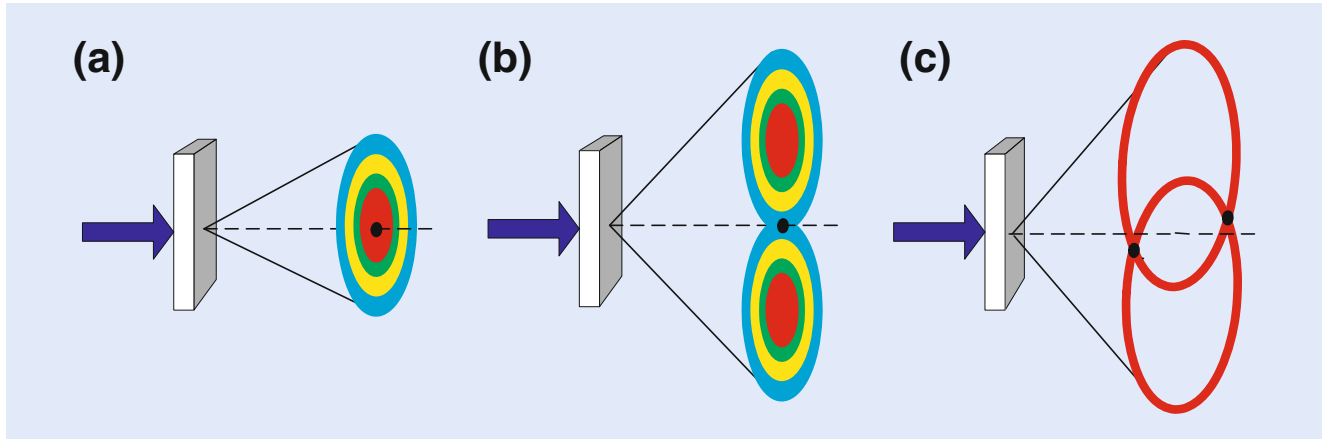


Fig. 16.3 Three widely used SPDC. (a) Type-I SPDC. (b) Collinear degenerate type-II SPDC. Two rings overlap at one region. (c) Non-collinear degenerate type-II SPDC. For clarity, only two degenerate rings, one for  $e$ -polarization and the other for  $o$ -polarization, are shown

$$|\Psi\rangle = \Psi_0 \int d\mathbf{k}_s d\mathbf{k}_i \delta[\omega_p - \omega_s(\mathbf{k}_s) - \omega_i(\mathbf{k}_i)] \times \delta(\mathbf{k}_p - \mathbf{k}_s - \mathbf{k}_i) a_s^\dagger(\mathbf{k}_s) a_i^\dagger(\mathbf{k}_i) |0\rangle \quad (16.16)$$

where  $\Psi_0$  is a normalization constant which has absorbed all omitted constants.

The way of achieving phase matching, i.e., the way of achieving the delta functions in Eq. (16.16) basically determines how the signal-idler pair “looks.” For example, in a negative uniaxial crystal, one can use a linearly polarized pump laser beam as an extraordinary ray of the crystal to generate a signal-idler pair both polarized as the ordinary rays of the crystal, which is defined as type-I phase matching. One can alternatively generate a signal-idler pair with one ordinary polarized and another extraordinary polarized, which is defined as type II phase matching. Figure 16.3 shows three examples of SPDC two-photon source. All three schemes have been widely used for different experimental purposes. Technical details can be found from textbooks and research references in nonlinear optics.

The two-photon state in the forms of Eq. (16.7) or Eq. (16.16) is a pure state, which describes the behavior of a signal-idler photon pair mathematically. Does the signal or the idler photon in the EPR state of Eq. (16.7) or Eq. (16.16) have a defined energy and momentum regardless of whether we measure it or not? Quantum mechanics answers: No! However, if one of the subsystems is measured with a certain energy and momentum, the other one is determined with certainty, despite the distance between them.

In the above calculation of the two-photon state we have approximated an infinite large volume of nonlinear interaction. For a finite volume of nonlinear interaction, we may write the state of the signal-idler photon pair in a more general form:

$$|\Psi\rangle = \int dk_s dk_i F(\mathbf{k}_s, \mathbf{k}_i) a_s^\dagger(\mathbf{k}_s) a_i^\dagger(\mathbf{k}_i) |0\rangle \quad (16.17)$$

where

$$\begin{aligned}
 F(\mathbf{k}_s, \mathbf{k}_i) &= \varepsilon \delta(\omega_p - \omega_s - \omega_i) f(\Delta_z L) h_{tr}(\vec{\kappa}_1 + \vec{\kappa}_2) \\
 f(\Delta_z L) &= \int_L dz e^{-i(k_p - k_{sz} - k_{iz})z} \\
 h_{tr}(\vec{\kappa}_1 + \vec{\kappa}_2) &= \int_A d\vec{\rho} \tilde{h}_{tr}(\vec{\rho}) e^{-i(\vec{\kappa}_s + \vec{\kappa}_i) \cdot \vec{\rho}} \\
 \Delta_z &= k_p - k_{sz} - k_{iz}
 \end{aligned} \tag{16.18}$$

where  $\varepsilon$  is named as parametric gain,  $\varepsilon$  is proportional to the second order electric susceptibility  $\chi^{(2)}$ , and is usually treated as a constant;  $L$  is the length of the nonlinear interaction; the integral in  $\vec{\kappa}$  is evaluated over the cross section  $A$  of the nonlinear material illuminated by the pump,  $\vec{\rho}$  is the transverse coordinate vector,  $\vec{\kappa}_j$  (with  $j = s, i$ ) is the transverse wavevector of the signal and idler, and  $f(|\vec{\rho}|)$  is the transverse profile of the pump, which can be treated as a Gaussian in most of the experimental conditions. The functions  $f(\Delta_z L)$  and  $h_{tr}(\vec{\kappa}_1 + \vec{\kappa}_2)$  can be approximated as  $\delta$ -functions for an infinitely long ( $L \sim \infty$ ) and wide ( $A \sim \infty$ ) nonlinear interaction region. The reason we have chosen the form of Eq. (16.18) is to separate the “longitudinal” and the “transverse” correlations. We will show that  $\delta(\omega_p - \omega_s - \omega_i)$  and  $f(\Delta_z L)$  together can be rewritten as a function of  $\omega_s - \omega_i$ . To simplify the mathematics, we assume near co-linearly SPDC. In this situation,  $|\vec{\kappa}_{s,i}| \ll |\mathbf{k}_{s,i}|$ .

Basically, function  $f(\Delta_z L)$  determines the “longitudinal” space-time correlation. Finding the solution of the integral is straightforward:

$$f(\Delta_z L) = \int_0^L dz e^{-i(k_p - k_{sz} - k_{iz})z} = e^{-i\Delta_z L/2} \text{sinc}(\Delta_z L/2). \tag{16.19}$$

where  $\text{sinc}(x) = \sin(x)/x$ .

Now, we consider  $f(\Delta_z L)$  with  $\delta(\omega_p - \omega_s - \omega_i)$  together, and taking advantage of the  $\delta$ -function in frequencies by introducing a detuning frequency  $\nu$  to evaluate function  $f(\Delta_z L)$ :

$$\begin{aligned}
 \omega_s &= \omega_s^0 + \nu \\
 \omega_i &= \omega_i^0 - \nu \\
 \omega_p &= \omega_s + \omega_i = \omega_s^0 + \omega_i^0.
 \end{aligned} \tag{16.20}$$

The dispersion relation  $k(\omega)$  allows us to express the wave numbers through the detuning frequency  $\nu$ :

$$\begin{aligned}
 k_s &\approx k(\omega_s^0) + \nu \left. \frac{dk}{d\omega} \right|_{\omega_s^0} = k(\omega_s^0) + \frac{\nu}{u_s}, \\
 k_i &\approx k(\omega_i^0) - \nu \left. \frac{dk}{d\omega} \right|_{\omega_i^0} = k(\omega_i^0) - \frac{\nu}{u_i}
 \end{aligned} \tag{16.21}$$

where  $u_s$  and  $u_i$  are group velocities for the signal and the idler, respectively. Now, we connect  $\Delta_z$  with the detuning frequency  $\nu$ :

$$\begin{aligned}
\Delta_z &= k_p - k_{sz} - k_{iz} \\
&= k_p - \sqrt{(k_s)^2 - (\vec{k}_s)^2} - \sqrt{(k_i)^2 - (\vec{k}_i)^2} \\
&\cong k_p - k_s - k_i + \frac{(\vec{k}_s)^2}{2k_s} + \frac{(\vec{k}_i)^2}{2k_i} \\
&\cong k_p - k(\omega_s^0) - k(\omega_i^0) + \frac{\nu}{u_s} - \frac{\nu}{u_i} + \frac{(\vec{k}_s)^2}{2k_s} + \frac{(\vec{k}_i)^2}{2k_i} \\
&\cong D\nu
\end{aligned} \tag{16.22}$$

where  $D \equiv 1/u_s - 1/u_i$ . We have also applied  $k_p - k(\omega_s^0) - k(\omega_i^0) = 0$  and  $|\vec{k}_{s,i}| \ll |\mathbf{k}_{s,i}|$ . The “longitudinal” wavevector correlation function is rewritten as a function of the detuning frequency  $\nu$ :  $f(\Delta_z L) \cong f(\nu DL)$ . In addition to the above approximations, we have inexplicitly assumed the angular independence of the wavevector  $k = n(\theta)\omega/c$ . For type II SPDC, the refraction index of the extraordinary-ray depends on the angle between the wavevector and the optical axis and an additional term appears in the expansion. Making the approximation valid, we have restricted our calculation to near-collinear process. Thus, for a good approximation, in the near-collinear experimental setup:

$$\Delta_z L \cong \nu DL = (\omega_s - \omega_i) DL/2. \tag{16.23}$$

Type-I degenerate SPDC is a special case. Due to the fact that  $u_s = u_i$ , and hence,  $D = 0$ , the expansion of  $k(\omega)$  should be carried out up to the second order. Instead of (16.23), we have

$$\Delta_z L \cong -\nu^2 D' L = -(\omega_s - \omega_i)^2 D' L/4 \tag{16.24}$$

where

$$D' \equiv \frac{d}{d\omega} \left( \frac{1}{u} \right) \Big|_{\omega^0}.$$

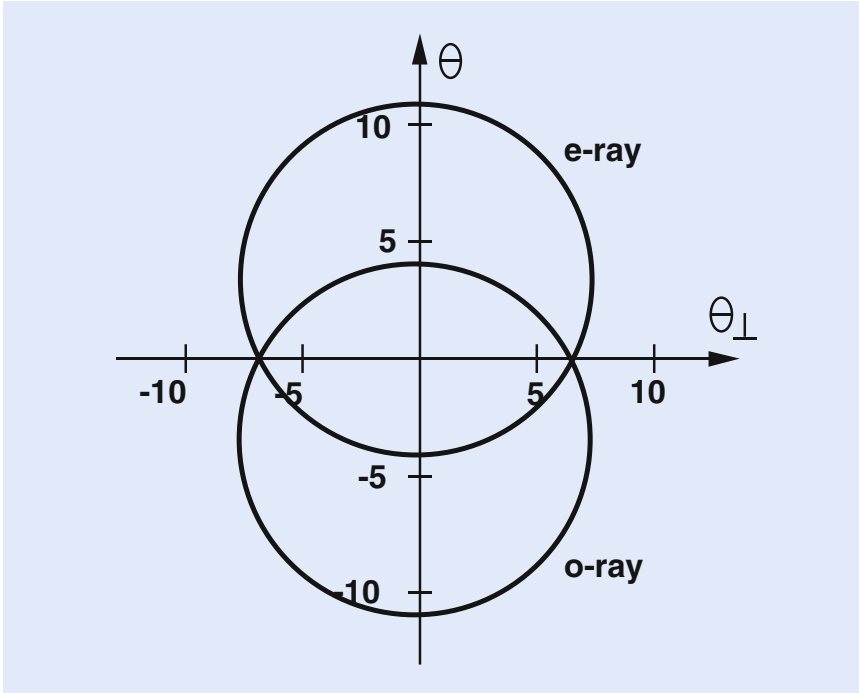
The two-photon state of the signal-idler pair is then approximated as

$$|\Psi\rangle = \int d\nu d\vec{k}_s d\vec{k}_i f(\nu) h_r(\vec{k}_s + \vec{k}_i) a_s^\dagger(\omega_s^0 + \nu, \vec{k}_s) a_i^\dagger(\omega_i^0 - \nu, \vec{k}_i) |0\rangle \tag{16.25}$$

where the normalization constant has been absorbed into  $f(\nu)$ .

SPDC has been one of the most convenient two-photon sources for the preparation of Bell state. Although Bell state is for polarization (or spin), the space-time part of the state cannot be ignored. One important “preparation” is to make the two biphoton wavepackets, corresponding to the first and the second terms in the Bell state, completely “overlap” in space-time, or indistinguishable for the joint detection event. This is especially important for type-II SPDC.

A very interesting situation for type-II SPDC is that of “noncollinear phase matching.” The signal-idler pair are emitted from an SPDC crystal, such as BBO, cut in type-II phase matching, into two cones, one ordinarily polarized, the other extraordinarily polarized, see Fig. 16.4. Along the intersection, where the cones overlap, two pinholes numbered 1 and 2 are used for defining the direction of the  $\mathbf{k}$  vectors of the signal-idler pair. It is very reasonable to consider the polarization state of the signal-idler pair as

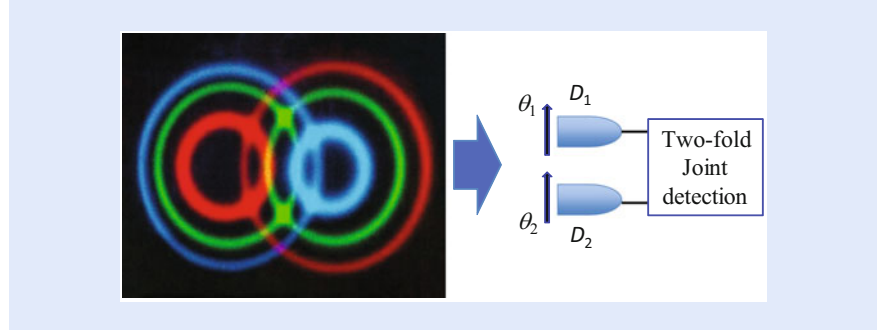


■ **Fig. 16.4** Type-II noncollinear phase matching: a cross section view of the degenerate 702.2 nm cones. The 351.1 nm pump beam is in the center. The numbers along the axes are in degrees

$$|\Psi\rangle = \frac{1}{\sqrt{2}}(|o_1e_2\rangle + |e_1o_2\rangle) = |\Psi^{(+)}\rangle \quad (16.26)$$

where  $o_j$  and  $e_j$ ,  $j = 1, 2$ , are ordinarily and extraordinarily polarization, respectively. It seems straightforward to realize an EPR-Bohm-Bell measurement by simply setting up a polarization analyzer in series with a photon counting detector behind pinholes 1 and 2, respectively, and to expect observe the polarization correlation. This is, however, *incorrect!* One can never observe the EPR-Bohm-Bell polarization correlation unless a “compensator” is applied [4]. The “compensator” is a piece of birefringent material. For example, one may place another piece of nonlinear crystal behind the SPDC. It could be the same type of crystal as that of the SPDC, with the same cutting angle, except having half the length and a  $90^\circ$  rotation with respect to that of the SPDC crystal.

What is the role of the “compensator”? There have been naive explanations about the compensator. One suggestion was that the problem comes from the longitudinal “walk-off” of the type-II SPDC. For example, if one uses a type II BBO, which is a negative uni-axis crystal, the extraordinary-ray propagates faster than the ordinary-ray inside the BBO. Suppose the  $o - e \leftrightarrow e - o$  pair is generated in the *middle* of the crystal, the  $e$ -polarization will trigger the detector earlier than the  $o$ -polarization by a time  $\Delta t = (n_o - n_e)L/2c$ . This implies that  $D_2$  would be fired first in  $|o_1e_2\rangle$  term; but  $D_1$  would be fired first in  $|e_1o_2\rangle$  term. If  $\Delta t$  is greater than the coherence length of the signal-idler field, one would be able to distinguish which amplitude gave rise to the “click-click” coincidence event. One may compensate the “walk-off” by introducing an additional piece of birefringent material, like the compensator we have suggested above, to delay the  $e$ -ray relative to the  $o$ -ray by the same amount of time,  $\Delta t$ . If, however, the signal-idler pair is generated in the *front face* or the *back face* of the SPDC, the delay time would be very



■ **Fig. 16.5** Schematic setup of a Bell correlation measurement. The orthogonally polarized signal-idler photon pair is created from type-II SPDC. The  $X$ -direction ( $Y$ -direction) is defined by the ordinary polarization (extraordinary polarization) of the nonlinear crystal

different:  $\Delta t = (n_o - n_e)L/c$  for the *front face* and  $\Delta t = 0$  for the *back face*. One can never satisfy all the pairs which are generated at different places along the SPDC crystal. Nevertheless, since SPDC is a *coherent* process, the signal-idler pair is generated in such a way that it is impossible to know the birthplace of the pair. So, how is the delay time  $\Delta t$  determined?

■ Figure 16.5 schematically illustrates a Bell correlation measurement in which an orthogonally polarized signal-idler photon pair of type-II SPDC is annihilated at  $(\mathbf{r}_1, t_1)$  and  $(\mathbf{r}_2, t_2)$  jointly by two point-like photon counting detectors  $D_1$  and  $D_2$  with two polarization analyzers oriented at  $\theta_1$  and  $\theta_2$ , respectively.

The coincidence counting rate of  $D_1$  and  $D_2$  measures the probability for a pair of photons to produce a joint photodetection event at  $D_1$  and  $D_2$ . In this setup, the pair has two different yet indistinguishable ways to produce a coincidence count: (1) the  $X$ -polarized photon passes  $\theta_1$  triggering  $D_1$ , the  $Y$ -polarized photon passes  $\theta_2$  triggering  $D_2$ ; (2) the  $Y$ -polarized photon passes  $\theta_1$  triggering  $D_1$ , the  $X$ -polarized photon passes  $\theta_2$  triggering  $D_2$ . If the above two alternatives are indistinguishable, quantum theory requires a superposition of the two probability amplitudes which results in an EPR-Bohm-Bell correlation:

$$R_c(\theta_1, \theta_2) \propto |\mathcal{A}_I(\theta_1, \theta_2) + \mathcal{A}_{II}(\theta_1, \theta_2)|^2 = \sin^2(\theta_1 + \theta_2). \quad (16.27)$$

To calculate the joint detection counting rate, we follow the Glauber formula [25]:

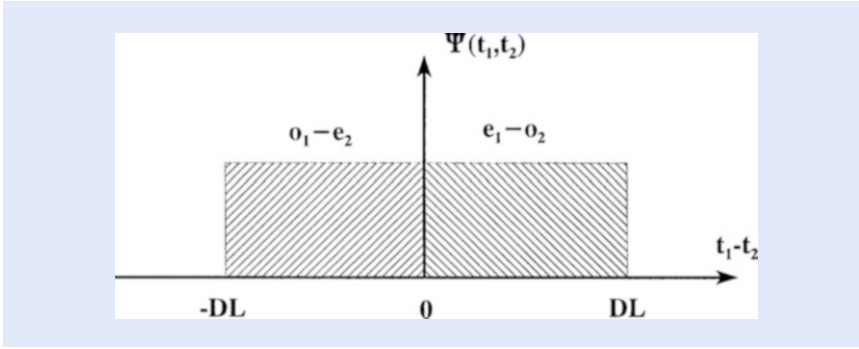
$$\begin{aligned} R_c &\propto \langle \Psi | E^{(-)}(\mathbf{r}_1, t_1) E^{(-)}(\mathbf{r}_2, t_2) E^{(+)}(\mathbf{r}_2, t_2) E^{(+)}(\mathbf{r}_1, t_1) | \Psi \rangle \\ &= |\langle 0 | E^{(+)}(\mathbf{r}_2, t_2) E^{(+)}(\mathbf{r}_1, t_1) | \Psi \rangle|^2. \end{aligned} \quad (16.28)$$

Adopting our earlier result, we may rewrite the state of the type-II signal-idler pair in the following form:

$$|\Psi\rangle = \int d\mathbf{k}_o d\mathbf{k}_e \delta(\omega_o + \omega_e - \omega_p) \Phi(\Delta_k L) \hat{\mathbf{o}} \cdot \hat{\mathbf{a}}_o^\dagger(\omega(\mathbf{k}_o)) \hat{\mathbf{e}} \cdot \hat{\mathbf{a}}_e^\dagger(\omega(\mathbf{k}_e)) |0\rangle \quad (16.29)$$

where  $\hat{\mathbf{o}}$  and  $\hat{\mathbf{e}}$  are unit vectors along the  $o$ -ray and the  $e$ -ray polarization direction of the SPDC crystal, and  $\Delta_k = k_o + k_e - k_p$ . In  $\Phi(\Delta_k L)$ , the finite length of the nonlinear crystal has been taken into account. Suppose the polarizers of the detectors  $D_1$  and  $D_2$  are set at angles  $\theta_1$  and  $\theta_2$ , relative to the polarization direction of the  $o$ -ray of the SPDC crystal, respectively, the field operators can be written as

$$E_j^{(+)}(t_j, \mathbf{r}_j) = \int d\omega \hat{\theta}_j a(\omega) e^{-i[\omega t_j - k(\omega) r_j]}$$



■ Fig. 16.6 Without “compensator,” the two dimensional wavepackets of  $\Psi(\tau_1^o, \tau_2^e)$  and  $\Psi(\tau_1^e, \tau_2^o)$  do not overlap along  $\tau_1 - \tau_2$  axis

where  $j = 1, 2$ ,  $\hat{\theta}_j$  is the unit vector along the orientation of the  $i$ th polarization analyzer. Substitute the field operator into Eq. (16.28),

$$\begin{aligned}
 R_c &\propto |(\hat{\theta}_1 \cdot \hat{\mathbf{o}})(\hat{\theta}_2 \cdot \hat{\mathbf{e}}) \Psi(\tau_1^o, \tau_2^e) + (\hat{\theta}_1 \cdot \hat{\mathbf{e}})(\hat{\theta}_2 \cdot \hat{\mathbf{o}}) \Psi(\tau_1^e, \tau_2^o)|^2 \\
 &= |\mathcal{A}_1(\theta_1, \theta_2) + \mathcal{A}_2(\theta_1, \theta_2)|^2 \\
 &= \cos^2 \theta_1 \sin^2 \theta_2 + \sin^2 \theta_1 \cos^2 \theta_2 \\
 &\quad + \cos \theta_1 \sin \theta_2 \sin \theta_1 \cos \theta_2 \Psi^*(\tau_1^o, \tau_2^e) \Psi(\tau_1^e, \tau_2^o)
 \end{aligned} \tag{16.30}$$

where  $\Psi(\tau_1^o, \tau_2^e)$  and  $\Psi(\tau_1^e, \tau_2^o)$  are the effective two-photon wavefunctions, namely the biphoton wavepackets, and  $\tau_j^o = t_j - r_j/u_o$ ,  $\tau_j^e = t_j - r_j/u_e$ . The third term of Eq. (16.30) determines the degree of two-photon coherence. Considering degenerate CW laser pumped SPDC, the biphoton wavepacket can be simplified as

$$\Psi(\tau_1, \tau_2) = \Psi_0 e^{-i\omega_p(\tau_1 + \tau_2)/2} \mathcal{F}_{\tau_-} \{f(\Omega)\}.$$

The coefficient of  $\cos \theta_1 \sin \theta_2 \sin \theta_1 \cos \theta_2$  in the third term of Eq. (16.30) is thus

$$e^{-i\omega_p(\Delta\tau_1 - \Delta\tau_2)/2} \mathcal{F}_{\tau_1^o - \tau_2^e} \{f(\Omega)\} \otimes \mathcal{F}_{\tau_1^e - \tau_2^o} \{f(\Omega)\}.$$

where  $\mathcal{F}_{\tau_-} \{f(\Omega)\}$  labels a Fourier transform.

Therefore, two important factors will determine the result of the polarization correlation measurement: (1) the phase of  $e^{-i\omega_p(\Delta\tau_1 - \Delta\tau_2)/2}$ ; and (2) the overlapping between the biphoton wavepackets  $\Psi^*(\tau_1^o, \tau_2^e)$  and  $\Psi(\tau_1^e, \tau_2^o)$ , i.e., the chances for both  $\Psi^*(\tau_1^o, \tau_2^e)$  and  $\Psi(\tau_1^e, \tau_2^o)$  take nonzero values simultaneously at  $\tau_1^o - \tau_2^e$ .

Examining the two wavepackets associated with the  $o_1 - e_2$  and  $e_1 - o_2$  terms, we found the two dimensional biphoton wavepackets of type II SPDC do not overlap, due to the *asymmetrical* rectangular function of  $\pi(\tau_1 - \tau_2)$  as indicated in ■ Fig. 16.6. In order to make the two wavepackets overlap, we may either (1) move both wavepackets a distance of  $DL/2$  (case I) or (2) move one of the wavepackets a distance of  $DL$  (case II). The use of “compensator” is for this purpose. After compensating the two asymmetrical function of  $\pi(\tau_1 - \tau_2)$ , we need to further manipulate the phase of  $e^{-i\omega_p(\Delta\tau_1 - \Delta\tau_2)/2}$  to finalize the desired Bell states. This can be done by means of a retardation plate to introduce phase delay of  $2\pi (+1)$  or  $\pi (-1)$  between the o-ray and the e-ray in either arm 1 or arm 2. The EPR-Bohm-Bell polarization correlation  $R_c \propto \sin^2(\theta_1 \pm \theta_2)$  is expected only when the above two conditions are satisfied. We can simplify the polarization state of the signal-idler photon pair in the form of Bell states  $|\Psi^{(\pm)}\rangle$  in this situation only.

In recent years, special attention has been paid to femtosecond laser pulse pumped SPDC due to its attractive applications in quantum information processing and communication. The biphoton wavepacket looks very different

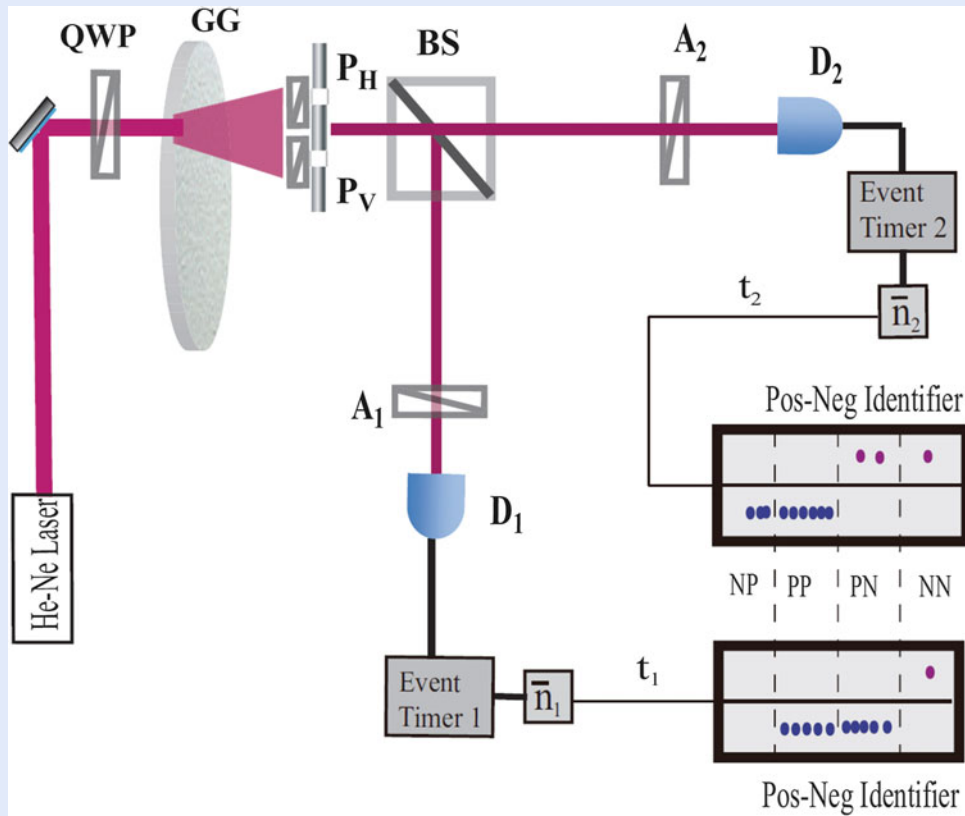


Fig. 16.7 Schematic setup of the experiment: polarization correlation measurement of thermal fields in photon-number fluctuations

in this case than that of the CW pump. One needs to examine the biphoton wavepackets carefully to be sure the superposed probability amplitudes overlap [26, 27].

From the above analysis, we may conclude the EPR-Bohm-Bell correlation is the result of a nonlocal interference: a pair of entangled photons interferes with the pair itself. This peculiar interference involves the superposition of two-photon wavepackets, or two-photon amplitudes, corresponding to different yet indistinguishable alternative ways for a pair of photons to produce a photodetection event at distant space-time coordinates.

### 16.2.2 Bell State Simulation of Thermal Light

Now we ask what would happen if we replace the entangled photons with a randomly paired photons, or wavepackets, in the thermal state? Can a randomly paired photons in a thermal state simulate the Bell state? The answer is positive. In the following we analyze a recent experiment of Peng et al. in which a Bell-type correlation was observed from the polarization measurement of thermal fields in photon-number fluctuations, indicating the successful simulation of Bell state [28]. Very importantly, the same mechanism can be easily extended to the simulation of a multi-photon GHZ state and  $N$ -qubits for  $N \gg 2$ .

Figure 16.7 schematically illustrates the experimental setup of Peng et al. A large number of circular polarized wavepackets at the single-photon level, such as the  $m$ th and the  $n$ th, come from a standard pseudo-thermal light source [29] consisting of a circularly polarized 633 nm CW laser beam and a rotating ground



glass (GG). The diameter of the laser beam is  $\sim 2$  mm. The size of the tiny diffusers on the GG is roughly a few micrometers. The randomly distributed wavepackets pass two pinholes  $P_H$  and  $P_V$  with two linear polarizers oriented at a horizontal polarization  $\vec{H}$  ( $\theta = 0^\circ$ ) and vertical polarization  $\vec{V}$  ( $\theta = 90^\circ$ ), respectively. The circular polarized wavepackets have 50 % chance to pass the upper pinhole  $P_H$  with horizontal polarization and 50 % chance to pass the lower pinhole  $P_V$  with vertical polarization. The separation between the two pinholes is much greater than the coherence length of the pseudo-thermal field. Therefore, (1) the  $\vec{H}$  polarization and  $\vec{V}$  polarization are first-order incoherent and the mixture of the two polarizations results in an unpolarized field; (2) the fluctuations of the  $\vec{H}$  polarization and the  $\vec{V}$  polarization are completely independent and random without any correlation. A 50–50 non-polarizing beamsplitter (BS) is used to divide the unpolarized thermal field, i.e., the 50–50 mixture of the two polarizations, into arms 1 and 2. Two polarization analyzers  $A_1$ , oriented at  $\theta_1$ , and  $A_2$ , oriented at  $\theta_2$ , followed by two photon counting detectors  $D_1$  and  $D_2$ , are placed into arms 1 and 2 for the measurement of the polarization of the wavepackets. The registration time and the number of photodetection events of  $D_1$  and  $D_2$  at each  $j$ th time window are recorded, respectively, by two independent but synchronized event timers. The width of the time window,  $\Delta t_j$ , can be adjusted from nanoseconds to milliseconds. For each detector,  $D_\beta$ ,  $\beta = 1, 2$ , at each chosen value of  $\theta_\beta$ , the mean photon number,  $\tilde{n}_\beta$ , is calculated from  $\tilde{n}_\beta = \left( \sum_{j=1}^N n_{\beta j} \right) / N$ ,

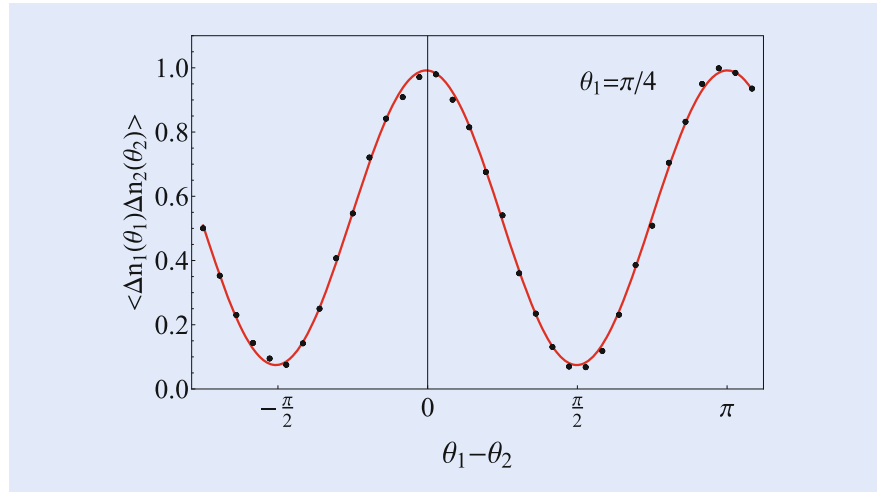
where  $N$  is the total number of time windows recorded for each data point in which  $\theta_1$  and  $\theta_2$  are set at certain chosen values. In our experiments, the total number and the width of the time window were  $N \approx 4 \times 10^5$ , and  $\Delta t_j = 800 \mu\text{s}$ . The mean photon number was chosen  $\tilde{n}_1 \sim \tilde{n}_2 \sim 20$ . In addition, the counting rate of  $D_1$  and  $D_2$  is monitored to be constants, independent of  $\theta_1$  and  $\theta_2$ . The number fluctuation is then calculated for each time window,  $\Delta n_{\beta j} = n_{\beta j} - \tilde{n}_\beta$  [30]:

$$\langle \Delta n_1(\theta_1) \Delta n_2(\theta_2) \rangle = \frac{1}{N} \left[ \sum_{j=1}^N \Delta n_{1j}(\theta_1) \Delta n_{2j}(\theta_2) \right]. \quad (16.31)$$

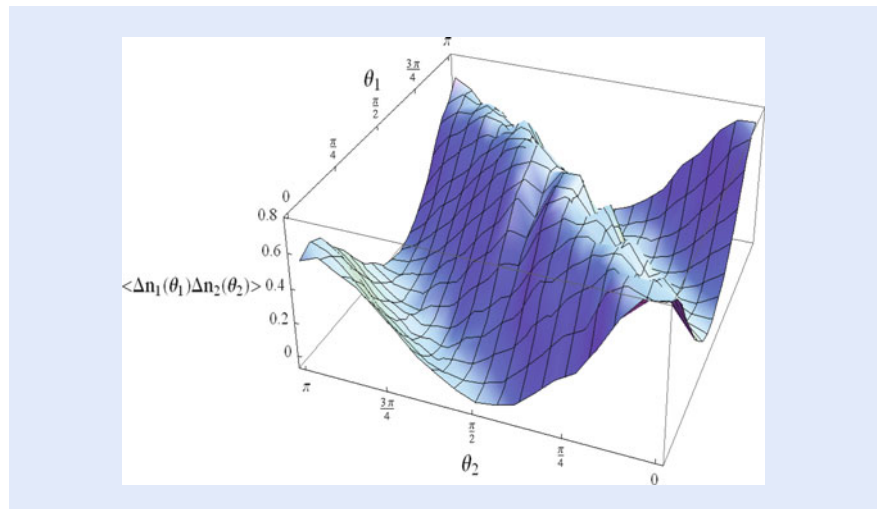
Achieving the maximum space-time correlation in photon-number fluctuations, we place  $D_1$  and  $D_2$  at equal longitudinal and transverse coordinates,  $z_1 = z_2$  and  $\vec{\rho}_1 = \vec{\rho}_2$ .

■ Figure 16.8 reports a typical measurement of the polarization correlation in photon-number fluctuation correlation. In this measurement, we fixed  $\theta_1 = 45^\circ$  and rotated  $\theta_2$  to a set of different values. The black dots are experimental data, the red sinusoidal curve is the theoretical fitting of  $\cos^2(\theta_1 - \theta_2)$  based on Eq. (16.44) with a  $\sim 92.5$  % contrast. For other values of  $\theta_1 \neq 45^\circ$  we have observed the same sinusoidal correlation function. ■ Figure 16.9 reports a measurement of  $\langle \Delta n_1(\theta_1) \Delta n_2(\theta_2) \rangle$  by scanning the values of  $\theta_1$  and  $\theta_2$  (2-D scanning). Based on these measurements, we conclude that our observed polarization correlation is the same as that of the Bell state  $|\Phi^{(+)}\rangle$ . Apparently, the post-selection measurements of the reported experiment has “entangled” a product state of polarization into the Bell state  $|\Phi^{(+)}\rangle$ .

To explain the experimental observation, we start from the analysis of chaotic-thermal light. Chaotic-thermal light may come from a natural thermal light source, such as the sun, or from a pseudo-thermal light source, usually consisting of a laser beam, either CW or pulsed, and a fast rotating ground glass containing a large number of tiny scattering diffusers (usually on the order of a few micrometers). For a natural thermal light source, each radiating atom among a large number of



■ **Fig. 16.8** Experimental observation of a Bell correlation with  $\sim 92.5\%$  contrast. The *black dots* are experimental data and the *red sinusoidal curve* is a theoretical fitting. The *horizontal axis* labels  $\varphi = \theta_1 - \theta_2$  while  $\theta_1$  was fixed at  $45^\circ$ , the *vertical axis* reports the normalized photon-number fluctuation correlation  $\langle \Delta n_1(\theta_1) \Delta n_2(\theta_2) \rangle$



■ **Fig. 16.9** A typical measurement of  $\langle \Delta n_1(\theta_1) \Delta n_2(\theta_2) \rangle$  by a 2-D scanning of  $\theta_1$  and  $\theta_2$

randomly distributed and randomly radiated atomic transitions can be considered a sub-source. A photon may be created from an atomic transition, or sub-source, such as the  $m$ th atomic transition, or the  $m$ th sub-source, at space-time coordinate  $(\mathbf{r}_{0m}, t_{0m})$ , where  $(\mathbf{r}_{0m})$  indicates the spatial coordinate of the  $m$ th atomic transition, and  $t_{0m}$  is the creation time of the photon. With a pseudo-thermal light source, each tiny scattering diffuser in the ground glass is a sub-source which scatters a wavepacket from the laser beam at space-time coordinate  $(\vec{\rho}_{0m}, t_{0m})$  with random phase  $\varphi_{0m}$ , where  $(\vec{\rho}_{0m})$  indicates the transverse spatial coordinates of the  $m$ th scattering diffuser of the fast rotating ground glass, and  $t_{0m}$  is the scattering time of the subfield. It is reasonable to model thermal light, either from a natural thermal light source or from a pseudo-thermal light source, in the coherence state representation [4, 31]:

$$|\Psi\rangle = \prod_m |\{\alpha_m\}\rangle = \prod_{m, \mathbf{k}} |\alpha_m(\mathbf{k})\rangle, \quad (16.32)$$

where  $m$  labels the  $m$ th photon that is created from the  $m$ th atomic transition of a natural thermal source, or the  $m$ th wavepacket that is scattered from the  $m$ th sub-source of the pseudo-thermal source, and  $\mathbf{k}$  is a wavevector.  $|\alpha_m(\mathbf{k})\rangle$  is an eigenstate of the annihilation operator with an eigenvalue  $\alpha_m(\mathbf{k})$ ,

$$\hat{a}_m(\mathbf{k})|\alpha_m(\mathbf{k})\rangle = \alpha_m(\mathbf{k})|\alpha_m(\mathbf{k})\rangle. \quad (16.33)$$

Thus, we have

$$\hat{a}_m(\mathbf{k})|\Psi\rangle = \alpha_m(\mathbf{k})|\Psi\rangle. \quad (16.34)$$

The field operator corresponding to the  $m$ th subfield at the detector can be written in the following form:

$$\hat{E}_m^{(+)}(\mathbf{r}, t) = \int d\omega \hat{a}_m(\omega) g_m(\omega; \mathbf{r}, t) \quad (16.35)$$

with  $g_m(\omega; \mathbf{r}, t)$  the Green's function that propagates the  $\omega$  mode of the  $m$ th subfield from the source to  $(\mathbf{r}, t)$ . A point-like photon counting detector, behind a polarizer oriented at angle  $\vec{\theta}$ , at space-time coordinate  $(\mathbf{r}, t)$  counts the photon number that is polarized along  $\vec{\theta}$ ,  $n(\theta; \mathbf{r}, t)$ , which is usually written as the sum of mean photon-number  $\langle n(\theta; \mathbf{r}, t) \rangle$  and the photon-number fluctuation  $\Delta n(\theta; \mathbf{r}, t)$ :

$$\begin{aligned} n(\theta; \mathbf{r}, t) &= \sum_m \vec{p}_m \langle \alpha_m | \sum_p \hat{E}_p^{(-)}(\mathbf{r}, t) \sum_q \hat{E}_q^{(+)}(\mathbf{r}, t) \sum_n \vec{p}_n | \alpha_n \rangle \\ &= \sum_m (\vec{p}_m \cdot \vec{\theta}) \Psi_m^*(\mathbf{r}, t) \sum_n (\vec{p}_n \cdot \vec{\theta}) \Psi_n(\mathbf{r}, t) \\ &= \sum_m (\vec{p}_m \cdot \vec{\theta}) \Psi_m^*(\mathbf{r}, t) (\vec{p}_m \cdot \vec{\theta}) \Psi_m(\mathbf{r}, t) \\ &\quad + \sum_{m \neq n} (\vec{p}_m \cdot \vec{\theta}) \Psi_m^*(\mathbf{r}, t) (\vec{p}_n \cdot \vec{\theta}) \Psi_n(\mathbf{r}, t) \\ &\equiv \sum_m \Psi_m^*(\theta; \mathbf{r}, t) \Psi_m(\theta; \mathbf{r}, t) + \sum_{m \neq n} \Psi_m^*(\theta; \mathbf{r}, t) \Psi_n(\theta; \mathbf{r}, t) \\ &= \langle n(\theta; \mathbf{r}, t) \rangle + \Delta n(\theta; \mathbf{r}, t), \end{aligned} \quad (16.36)$$

where  $\vec{p}_m$  is the polarization of the  $m$ th wavepacket,  $|\alpha_m\rangle$  is the state of the  $m$ th photon or the  $m$ th group of identical photons in the thermal state. In Eq. (16.36) we have introduced the effective wavefunction of a photon or a group of identical photons:

$$\Psi_m(\mathbf{r}, t) = \langle \alpha_m | \hat{E}_m^{(+)}(\mathbf{r}, t) | \alpha_m \rangle = \int d\omega a_m(\omega) g_m(\omega; \mathbf{r}, t). \quad (16.37)$$

An effective wavefunction or a wavepacket, corresponding to the classical concept of an electromagnetic subfield  $\mathbf{E}_m(\mathbf{r}, t)$  however, represents a very different physical reality. The effective wavefunction represents the “probability amplitude” for a photon or a group of identical photons to produce a photoelectron event at space-time coordinate  $(\mathbf{r}, t)$ . From Eq. (16.36), we find that the mean photon-number  $\langle n(\theta; \mathbf{r}, t) \rangle = \sum_m \Psi_m^*(\theta; \mathbf{r}, t) \Psi_m(\theta; \mathbf{r}, t)$  involves the effective wavefunction of a

photon or a wavepacket while the photon-number fluctuation  $\Delta n(\theta; \mathbf{r}, t) =$

$\sum_{m \neq n} \Psi_m^*(\theta; \mathbf{r}, t) \Psi_n(\theta; \mathbf{r}, t)$  involves the effective wave functions of two different photons, or a random pair of wavepackets,  $m \neq n$ . The measurement of mean

photon-number gives the self-coherence of a photon or a group of identical photons while the measurement of photon-number fluctuation gives the mutual-coherence between different photons or different groups of identical photons. In the polarization-based photon counting measurement, the above equation can be used to calculate either the polarization correlation or the space-time correlation.

In general, a Bell type experiment measures the statistical correlation between  $n(\theta_1; \mathbf{r}_1, t_1)$  and  $n(\theta_2; \mathbf{r}_2, t_2)$ . For thermal light, the photon-number correlation can be written as the sum of two contributions [4]:

$$\begin{aligned} \langle n_1(\theta_1)n_2(\theta_2) \rangle &= \langle n_1(\theta_1) \rangle \langle n_2(\theta_2) \rangle + \langle \Delta n_1(\theta_1) \Delta n_2(\theta_2) \rangle \\ &= \sum_m \Psi_{m1}^* \Psi_{m1} \sum_n \Psi_{n2}^* \Psi_{n2} + \sum_{m \neq n} \Psi_{m1}^* \Psi_{n1} \Psi_{n2}^* \Psi_{m2}. \end{aligned} \quad (16.38)$$

Here, we have shortened the notations of the effective wavefunction: the subindex  $\beta$ ,  $\beta = 1, 2$ , indicates  $\theta_\beta$  and  $(\mathbf{r}_\beta, t_\beta)$ . The first contribution is the result of two independent mean photon-number measurements, the statistics and coherence involves the measurement of single photons only while the second contribution is the result of photon-number fluctuation correlation, the statistics and coherence involves randomly paired photons. A Bell type experiment studies the polarization correlation of a pair of photons, obviously, we need to measure the photon-number fluctuation correlation  $\langle \Delta n_1(\theta_1) \Delta n_2(\theta_2) \rangle$ . The measurement of  $\langle \Delta n_1(\theta_1) \Delta n_2(\theta_2) \rangle$  gives both polarization correlation and space-time correlation between two randomly paired photons. In the Bell type measurements, we usually manage to achieve a maximum correlation in space-time, then test the polarization correlation  $\langle \Delta n_1(\theta_1) \Delta n_2(\theta_2) \rangle$  as a function of  $\varphi = \theta_1 - \theta_2$  by varying  $\theta_1$  and  $\theta_2$  to all possible different values.

The effective wavefunctions:  $\Psi_{m1}^*$ ,  $\Psi_{n1}$ ,  $\Psi_{n2}^*$ , and  $\Psi_{m2}$  are calculated in the flowing. In general, each operator of the subfield is identified to be

$$\hat{E}_{m\beta}^{(+)} = \int d\omega \hat{a}_m(\omega) g_m(\omega; \mathbf{r}_\beta, t_\beta). \quad (16.39)$$

Examine the experiment detail, we find

$$\begin{aligned} g_m(\omega; \mathbf{r}_\beta, t_\beta) &= \frac{1}{\sqrt{2}} \left[ (\vec{H} \cdot \vec{\theta}_\beta) g_m(\omega; \mathbf{r}_H, t_H) g_H(\omega; \mathbf{r}_\beta, t_\beta) \right. \\ &\quad \left. + (\vec{V} \cdot \vec{\theta}_\beta) g_m(\omega; \mathbf{r}_V, t_V) g_V(\omega; \mathbf{r}_\beta, t_\beta) \right], \end{aligned} \quad (16.40)$$

where  $g_m(\omega; \mathbf{r}_H, t_H)$  and  $g_H(\omega; \mathbf{r}_\beta, t_\beta)$  are the Green's functions that propagate the  $\omega$  mode of the  $m$ th subfield from the source to the upper pinhole  $P_H$  and from  $P_H$  to  $D_\beta$ , respectively. The effective wavefunction  $\Psi_{m\beta}$  is thus

$$\begin{aligned} \Psi_{m\beta} &= \int d\omega a_m \frac{1}{\sqrt{2}} \left[ (\vec{H} \cdot \vec{\theta}_\beta) g_m(\omega; \mathbf{r}_H, t_H) g_{P_H}(\omega; \mathbf{r}_\beta, t_\beta) \right. \\ &\quad \left. + (\vec{V} \cdot \vec{\theta}_\beta) g_m(\omega; \mathbf{r}_V, t_V) g_{P_V}(\omega; \mathbf{r}_\beta, t_\beta) \right] \\ &= \frac{1}{\sqrt{2}} [\Psi_{mH\beta} + \Psi_{mV\beta}], \end{aligned} \quad (16.41)$$

where  $\Psi_{mH\beta}$  is the  $m$ th wavepacket passes  $P_H$ ,  $\theta_\beta$ , triggers  $D_\beta$ , and  $\Psi_{mV\beta}$  the  $m$ th wavepacket passes  $P_V$ ,  $\theta_\beta$ , triggers  $D_\beta$ . The normalized photon-number fluctuation correlation is thus

$$\begin{aligned}
\langle \Delta n_1(\theta_1) \Delta n_2(\theta_2) \rangle &= \sum_{m,n} \Psi_{m1}^* \Psi_{n1} \Psi_{m2} \Psi_{n2}^* \\
&= \sum_{m,n} \frac{1}{\sqrt{2}} [\Psi_{mH1}^* + \Psi_{mV1}^*] \frac{1}{\sqrt{2}} [\Psi_{nH1} + \Psi_{nV1}] \quad (16.42) \\
&\quad \times \frac{1}{\sqrt{2}} [\Psi_{mH2} + \Psi_{mV2}] \frac{1}{\sqrt{2}} [\Psi_{nH2}^* + \Psi_{nV2}^*]
\end{aligned}$$

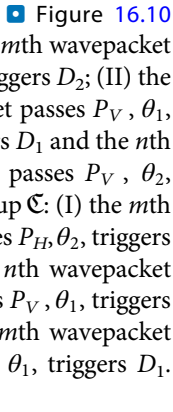
where, for example,  $\Psi_{mH1}$  is the  $m$ th wavepacket passing through the upper pinhole with  $\vec{H}$  polarization contributing to the photodetection event of  $D_1$  at space-time  $(\mathbf{r}_1, t_1)$ . In this experiment, we have separated the pinholes  $P_H$  and  $P_V$  beyond the transverse coherence length of the thermal field. Therefore, only four of the above sixteen terms survive from the sum of  $m$  and  $n$ ,

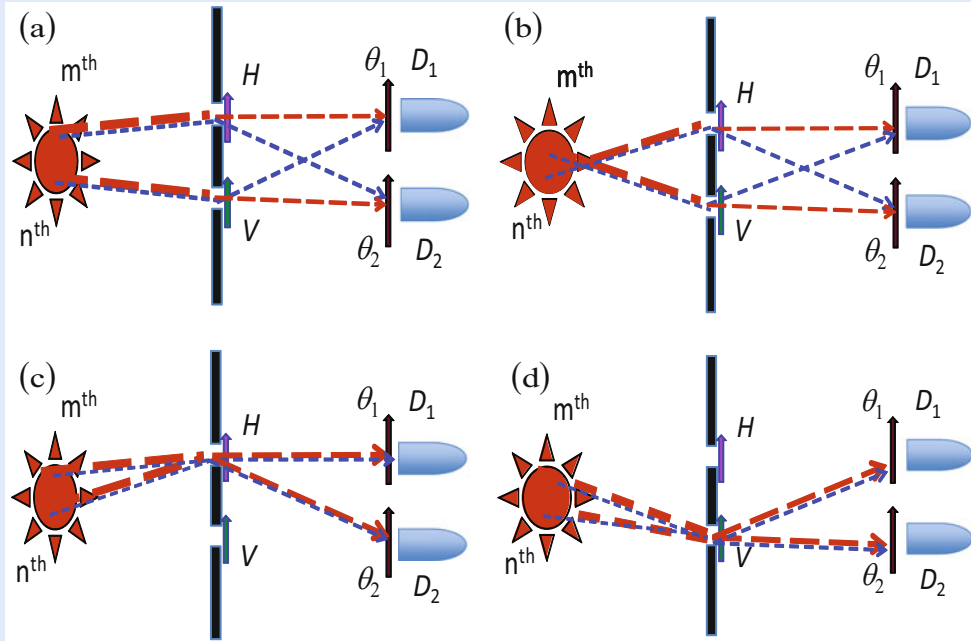
$$\begin{aligned}
\langle \Delta n_1(\theta_1) \Delta n_2(\theta_2) \rangle &\propto \sum_{m,n} [\Psi_{mH1}^* \Psi_{mH2} \Psi_{nH1} \Psi_{nH2}^* + \Psi_{mH1}^* \Psi_{mH2} \Psi_{nV1} \Psi_{nV2}^* \quad (16.43) \\
&\quad + \Psi_{mV1}^* \Psi_{mV2} \Psi_{nH1} \Psi_{nH2}^* + \Psi_{mV1}^* \Psi_{mV2} \Psi_{nV1} \Psi_{nV2}^*]
\end{aligned}$$

corresponding to an interference effect which involves the joint detection of two wavepackets at two independent photodetectors located a distance apart. Adding the four cross terms that involve the random pair, i.e., the  $m$ th and the  $n$ th wavepackets, which is observable in the photon-number fluctuations, we obtain

$$\begin{aligned}
\langle \Delta n_1(\theta_1) \Delta n_2(\theta_2) \rangle &\propto [\cos \theta_1 \cos \theta_2 \cos \theta_1 \cos \theta_2 + \cos \theta_1 \cos \theta_2 \sin \theta_1 \sin \theta_2 \\
&\quad + \sin \theta_1 \sin \theta_2 \cos \theta_1 \cos \theta_2 + \sin \theta_1 \sin \theta_2 \sin \theta_1 \sin \theta_2] \quad (16.44) \\
&= |\cos \theta_1 \cos \theta_2 + \sin \theta_1 \sin \theta_2|^2 \\
&= \cos^2(\theta_1 - \theta_2),
\end{aligned}$$

which is the same correlation as that of the Bell state  $|\Phi^{(+)}\rangle$ .

Under the experimental condition of equal transverse and longitudinal (temporal) coordinates of  $D_1$  and  $D_2$ , the observed correlation is the result of four groups of nonlocal superposition between different yet indistinguishable probability amplitudes of a randomly paired photons, or wavepackets. 



16

Fig. 16.10 There exist four groups of different yet indistinguishable amplitudes of the  $m$ th and the  $n$ th wavepacket to produce a joint photodetector event

$$\begin{aligned}
 |\mathcal{A}_I(\theta_1, \theta_2) + \mathcal{A}_{II}(\theta_1, \theta_2)|^2 &= |\Psi_{mH1}\Psi_{nV2} + \Psi_{mH2}\Psi_{nV1}|^2 \\
 |\mathcal{B}_I(\theta_1, \theta_2) + \mathcal{B}_{II}(\theta_1, \theta_2)|^2 &= |\Psi_{mV1}\Psi_{nH2} + \Psi_{mV2}\Psi_{nH1}|^2 \\
 |\mathcal{C}_I(\theta_1, \theta_2) + \mathcal{C}_{II}(\theta_1, \theta_2)|^2 &= |\Psi_{mH1}\Psi_{nH2} + \Psi_{mH2}\Psi_{nH1}|^2 \\
 |\mathcal{D}_I(\theta_1, \theta_2) + \mathcal{D}_{II}(\theta_1, \theta_2)|^2 &= |\Psi_{mV1}\Psi_{nV2} + \Psi_{mV2}\Psi_{nV1}|^2.
 \end{aligned} \tag{16.45}$$

Adding the four cross terms that involve the random pair, i.e., the  $m$ th and the  $n$ th wavepackets, which is observable in the photon-number fluctuations, we obtain Eq. (16.44).

### 16.2.3 Bell's Inequality

In 1964, Bell derived an inequality to distinguish quantum mechanics from local realistic probability theory of hidden variable [32]. In his pioneer work Bell introduced a “more complete specification effected by means of parameter  $\lambda$ ” with probability distribution  $\rho(\lambda)$  for the classical statistical estimation of the expectation value of the spin correlation measurement  $\langle \Psi | (\vec{\sigma}_1 \cdot \hat{\mathbf{a}}) (\vec{\sigma}_2 \cdot \hat{\mathbf{b}}) | \Psi \rangle$  of particle-1 and particle-2, such as the spin-1/2 particle pair of Bohm, in the directions  $\hat{\mathbf{a}}$  and  $\hat{\mathbf{b}}$ , simultaneously and respectively. The quantum mechanical result of this measurement gives

$$E_{ab} = \langle \Psi | (\vec{\sigma}_1 \cdot \hat{\mathbf{a}}) (\vec{\sigma}_2 \cdot \hat{\mathbf{b}}) | \Psi \rangle = -\hat{\mathbf{a}} \cdot \hat{\mathbf{b}}. \quad (16.46)$$

A special case of this result contains the determinism implicit in this idealized system. When the Stern–Gerlach analyzers (SGA) are parallel, we have

$$E_{ab} = \langle \Psi | (\vec{\sigma}_1 \cdot \hat{\mathbf{a}}) (\vec{\sigma}_2 \cdot \hat{\mathbf{a}}) | \Psi \rangle = -1 \quad (16.47)$$

for all  $\lambda$  and all  $\hat{\mathbf{a}}$ . Thus, we can predict with certainty the result B by obtaining the result of A. Since  $|\Psi\rangle$  does not determine the result of an individual measurement, this fact (via EPR's argument) suggests that there exists a more complete specification of the state by a single symbol  $\lambda$  it may have many dimensions, discrete and/or continuous parts, and different parts of it interacting with either apparatus, etc. Let  $\Lambda$  be the space of  $\lambda$  for an ensemble composed of a very large number of the particle systems. Bell represented the distribution function for the state  $\lambda$  on the space  $\Lambda$  by the symbol  $\rho(\lambda)$  and take  $\rho(\lambda)$  to be normalized

$$\int_{\Lambda} \rho(\lambda) d\lambda = 1. \quad (16.48)$$

In a deterministic hidden variable theory the observable  $[A(\hat{\mathbf{a}})B(\hat{\mathbf{b}})]$  has a defined value  $[A(\hat{\mathbf{a}})B(\hat{\mathbf{b}})](\lambda)$  for the state  $\lambda$ .

The locality is defined as follows: a deterministic hidden variable theory is local if for all  $\hat{\mathbf{a}}$  and  $\hat{\mathbf{b}}$  and all  $\lambda \in \Lambda$

$$[A(\hat{\mathbf{a}})B(\hat{\mathbf{b}})](\lambda) = A(\hat{\mathbf{a}}, \lambda) B(\hat{\mathbf{b}}, \lambda). \quad (16.49)$$

This is, once  $\lambda$  is specified and the particle has separated, measurements of A can depend only upon  $\lambda$  and  $\hat{\mathbf{a}}$  but not  $\hat{\mathbf{b}}$ . Likewise measurements of B depend only upon  $\lambda$  and  $\hat{\mathbf{b}}$ . Any reasonable physical theory that is realistic and deterministic and that denies action-at-a-distance is local in this sense. For such theories the expectation value of  $[A(\hat{\mathbf{a}})B(\hat{\mathbf{b}})]$  is given by

$$\begin{aligned} E(\hat{\mathbf{a}}, \hat{\mathbf{b}}) &= \int_{\Lambda} d\lambda \rho(\lambda) [A(\hat{\mathbf{a}})B(\hat{\mathbf{b}})](\lambda) \\ &= \int_{\Lambda} d\lambda \rho(\lambda) A(\hat{\mathbf{a}}, \lambda) B(\hat{\mathbf{b}}, \lambda), \end{aligned} \quad (16.50)$$

where  $E(\hat{\mathbf{a}}, \hat{\mathbf{b}}) \equiv E_{ab}$ , corresponding to our previous notation. It is clear that Eq. (16.47) can hold if only if

$$A(\hat{\mathbf{a}}, \lambda) = -B(\hat{\mathbf{b}}, \lambda) \quad (16.51)$$

hold for all  $\lambda \in \Lambda$ .

Using Eq. (16.51) we calculate the following expectation values, which involves three different orientations of the SGA analyzers:

$$\begin{aligned}
E(\hat{\mathbf{a}}, \hat{\mathbf{b}}) - E(\hat{\mathbf{a}}, \hat{\mathbf{c}}) &= \int_{\Lambda} d\lambda \rho(\lambda) [A(\hat{\mathbf{a}}, \lambda) B(\hat{\mathbf{b}}, \lambda) - A(\hat{\mathbf{a}}, \lambda) B(\hat{\mathbf{c}}, \lambda)] \\
&= - \int_{\Lambda} d\lambda \rho(\lambda) [A(\hat{\mathbf{a}}, \lambda) A(\hat{\mathbf{b}}, \lambda) - A(\hat{\mathbf{a}}, \lambda) A(\hat{\mathbf{c}}, \lambda)] \\
&= - \int_{\Lambda} d\lambda \rho(\lambda) A(\hat{\mathbf{a}}, \lambda) A(\hat{\mathbf{b}}, \lambda) [1 - A(\hat{\mathbf{b}}, \lambda) A(\hat{\mathbf{c}}, \lambda)].
\end{aligned} \tag{16.52}$$

Since  $A(\hat{\mathbf{a}}, \lambda) = \pm 1$ ,  $A(\hat{\mathbf{b}}, \lambda) = \pm 1$ , this expression can be written as

$$|E(\hat{\mathbf{a}}, \hat{\mathbf{b}}) - E(\hat{\mathbf{a}}, \hat{\mathbf{c}})| \leq \int_{\Lambda} d\lambda \rho(\lambda) [1 - A(\hat{\mathbf{b}}, \lambda) A(\hat{\mathbf{c}}, \lambda)], \tag{16.53}$$

and consequently,

$$|E(\hat{\mathbf{a}}, \hat{\mathbf{b}}) - E(\hat{\mathbf{a}}, \hat{\mathbf{c}})| \leq 1 + E(\hat{\mathbf{b}}, \hat{\mathbf{c}}). \tag{16.54}$$

This inequality is the first of a family of inequalities which are collectively called ‘‘Bell’s inequalities.’’

It is easy to find a disagreement between the quantum mechanics prediction of Eq. (16.46) and the inequality of Eq. (16.54). When we choose  $\hat{\mathbf{a}}$ ,  $\hat{\mathbf{b}}$ , and  $\hat{\mathbf{c}}$  to be coplanar with  $\hat{\mathbf{c}}$  making an angle of  $2\pi/3$  with  $\hat{\mathbf{a}}$ , and  $\hat{\mathbf{b}}$  making an angle of  $\pi/3$  with both  $\hat{\mathbf{a}}$  and  $\hat{\mathbf{c}}$ , the quantum prediction gives

$$|[E(\hat{\mathbf{a}}, \hat{\mathbf{b}}) - E(\hat{\mathbf{a}}, \hat{\mathbf{c}})]_{QM}| = 1, \tag{16.55}$$

while

$$1 + [E(\hat{\mathbf{b}}, \hat{\mathbf{c}})]_{QM} = \frac{1}{2}. \tag{16.56}$$

It does not satisfy inequality of Eq. (16.54).

It was soon realized that the Bell’s inequality of Eq. (16.54) cannot be tested in a real experiment. Because Eq. (16.47) cannot be realized exactly in a realistic measurement. Any real detector cannot have a perfect quantum efficiency of 100 %, and any real analyzer cannot have a perfect distinguish ratio between orthogonal channels. In 1971, Bell proved a new inequality [33] which includes these concerns by assuming the outcomes of measurement A or B may take one of the following possible results:

$$A(\hat{\mathbf{a}}, \lambda) \text{ or } B(\hat{\mathbf{b}}, \lambda) = \begin{cases} +1 & \text{‘‘spin – up’’} \\ -1 & \text{‘‘spin – down’’} \\ 0 & \text{particle not detected} \end{cases} \tag{16.57}$$

For a given state  $\lambda$ , we define the measured values for these quantities by the symbols  $\bar{A}(\hat{\mathbf{a}}, \lambda)$  and  $\bar{B}(\hat{\mathbf{b}}, \lambda)$ , which satisfy

$$|\bar{A}(\hat{\mathbf{a}}, \lambda)| \leq 1 \quad \text{and} \quad |\bar{B}(\hat{\mathbf{b}}, \lambda)| \leq 1. \tag{16.58}$$



Following the same definition of locality, the expectation value of  $A(\hat{\mathbf{a}})B(\hat{\mathbf{b}})$  is calculated as

$$E(\hat{\mathbf{a}}, \hat{\mathbf{b}}) = \int_{\Lambda} d\lambda \rho(\lambda) \bar{A}(\hat{\mathbf{a}}, \lambda) \bar{B}(\hat{\mathbf{b}}, \lambda). \quad (16.59)$$

Consider a measurement which involves  $E(\hat{\mathbf{a}}, \hat{\mathbf{b}})$  and  $E(\hat{\mathbf{a}}, \hat{\mathbf{b}}')$

$$\begin{aligned} & E(\hat{\mathbf{a}}, \hat{\mathbf{b}}) - E(\hat{\mathbf{a}}, \hat{\mathbf{b}}') \\ &= \int_{\Lambda} d\lambda \rho(\lambda) [\bar{A}(\hat{\mathbf{a}}, \lambda) \bar{B}(\hat{\mathbf{b}}, \lambda) - \bar{A}(\hat{\mathbf{a}}, \lambda) \bar{B}(\hat{\mathbf{b}}', \lambda)], \end{aligned} \quad (16.60)$$

which can be written in the following form:

$$\begin{aligned} & E(\hat{\mathbf{a}}, \hat{\mathbf{b}}) - E(\hat{\mathbf{a}}, \hat{\mathbf{b}}') \\ &= \int_{\Lambda} d\lambda \rho(\lambda) \bar{A}(\hat{\mathbf{a}}, \lambda) \bar{B}(\hat{\mathbf{b}}, \lambda) [1 \pm \bar{A}(\hat{\mathbf{a}}', \lambda) \bar{B}(\hat{\mathbf{b}}', \lambda)] \\ &\quad - \int_{\Lambda} d\lambda \rho(\lambda) \bar{A}(\hat{\mathbf{a}}, \lambda) \bar{B}(\hat{\mathbf{b}}', \lambda) [1 \pm \bar{A}(\hat{\mathbf{a}}', \lambda) \bar{B}(\hat{\mathbf{b}}, \lambda)]. \end{aligned} \quad (16.61)$$

Applying the triangle theorem, and considering  $\rho(\lambda)[1 \pm \bar{A}(\hat{\mathbf{a}}', \lambda)\bar{B}(\hat{\mathbf{b}}', \lambda)]$  and  $\rho(\lambda)[1 \pm \bar{A}(\hat{\mathbf{a}}', \lambda)\bar{B}(\hat{\mathbf{b}}, \lambda)]$  cannot take negative values, then using inequality in Eq. (16.58), we obtain

$$\begin{aligned} |E(\hat{\mathbf{a}}, \hat{\mathbf{b}}) - E(\hat{\mathbf{a}}, \hat{\mathbf{b}}')| &\leq \int_{\Lambda} d\lambda \rho(\lambda) [1 \pm \bar{A}(\hat{\mathbf{a}}', \lambda) \bar{B}(\hat{\mathbf{b}}', \lambda)] \\ &\quad + \int_{\Lambda} d\lambda \rho(\lambda) [1 \pm \bar{A}(\hat{\mathbf{a}}', \lambda) \bar{B}(\hat{\mathbf{b}}, \lambda)], \end{aligned} \quad (16.62)$$

or

$$|E(\hat{\mathbf{a}}, \hat{\mathbf{b}}) - E(\hat{\mathbf{a}}, \hat{\mathbf{b}}')| \leq \pm [E(\hat{\mathbf{a}}', \hat{\mathbf{b}}') + E(\hat{\mathbf{a}}', \hat{\mathbf{b}})] + 2 \int_{\Lambda} d\lambda \rho(\lambda). \quad (16.63)$$

We thus derive a measurable inequality

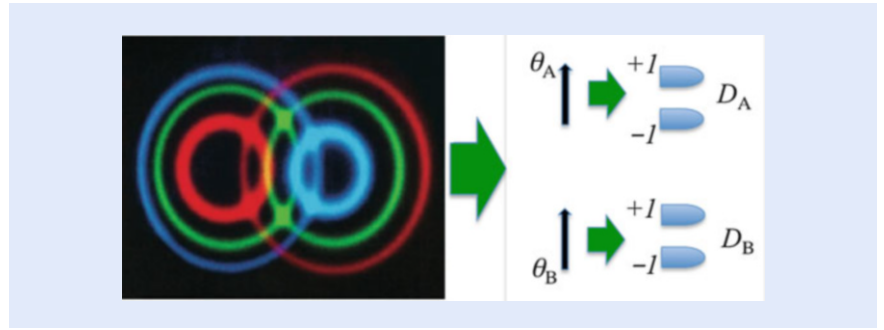
$$-2 \leq E(\hat{\mathbf{a}}, \hat{\mathbf{b}}) - E(\hat{\mathbf{a}}, \hat{\mathbf{b}}') + E(\hat{\mathbf{a}}', \hat{\mathbf{b}}) + E(\hat{\mathbf{a}}', \hat{\mathbf{b}}') \leq 2. \quad (16.64)$$

The quantum mechanical prediction of the EPR-Bhom state in a realistic measurement with imperfect detectors, analyzers etc., can be written as

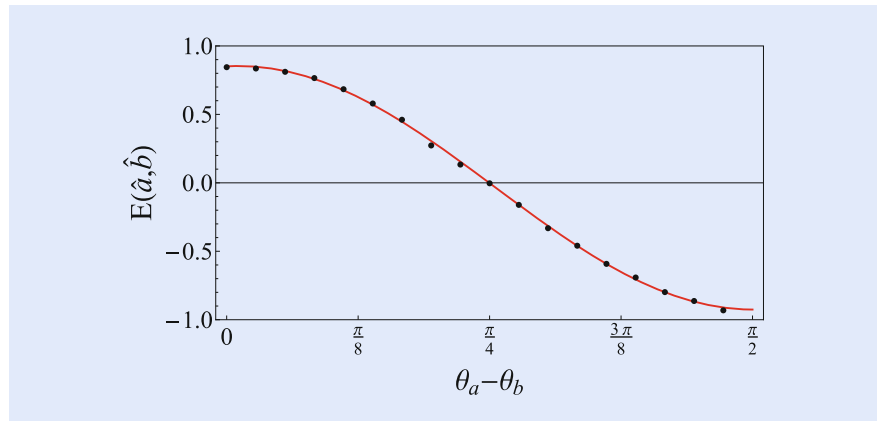
$$[E(\hat{\mathbf{a}}, \hat{\mathbf{b}})]_{QM} = C \hat{\mathbf{a}} \cdot \hat{\mathbf{b}} \quad (16.65)$$

where  $|C| \leq 1$ . Suppose we take  $\hat{\mathbf{a}}, \hat{\mathbf{a}}', \hat{\mathbf{b}}, \hat{\mathbf{b}}'$  to be coplanar with  $\phi = \pi/4$ , we can easily find a disagreement between the quantum mechanics prediction and the inequality of Eq. (16.64):

$$[E(\hat{\mathbf{a}}, \hat{\mathbf{b}}) - E(\hat{\mathbf{a}}, \hat{\mathbf{b}}') + E(\hat{\mathbf{a}}', \hat{\mathbf{b}}) + E(\hat{\mathbf{a}}', \hat{\mathbf{b}}')]_{QM} = 2\sqrt{2} C. \quad (16.66)$$



■ Fig. 16.11 Schematic setup of a Bell's inequality measurement. The expectation value is calculated from Eq. (16.67) which involves the measurement of four joint photodetections of  $D_A^+ & D_B^+$ ,  $D_A^- & D_B^+$ ,  $D_A^+ & D_B^-$ , and  $D_A^- & D_B^-$



■ Fig. 16.12 Experimental observation of  $E(\theta_A, \theta_B)$  from a typical Bell's inequality measurement. The black dots are experimental data and the red sinusoidal curve is a theoretical fitting

Although Bell derived his inequalities based on the measurement of spin-1/2 particle pairs, Eqs. (16.54) and (16.64) are not restricted to the measurement of spin-1/2 particle pairs. In fact, most of the historical experimental testing have been the polarization measurements of photon pairs. The photon pairs are prepared in similar states which have been called EPR-Bohm-Bell states, or Bell states in short. Most of the experimental observations violated Bell's inequalities which may have different forms and have their violation occur at different orientations of the polarization analyzers. However, the physics behind the violations is all similar to that of Bell's theorem.

■ Figure 16.11 is a schematic experimental setup for a Bell's inequality measurement. Since the space of  $\Lambda$  in this measurement is spanned into four regions with classical probabilities  $P_{ab}$ ,  $P_{-ab}$ ,  $P_{a-b}$ ,  $P_{-a-b}$  in which A and B have values  $\pm 1$ , the expectation value evaluation of Eq. (16.50) can be explicitly calculated as

$$E_{ab} = (+1)(+1)P_{ab} + (-1)(+1)P_{-ab} + (+1)(-1)P_{a-b} + (-1)(-1)P_{-a-b} = P_{ab} - P_{-ab} - P_{a-b} + P_{-a-b}, \tag{16.67}$$

$P_{ab}$ ,  $P_{-ab}$ ,  $P_{a-b}$  and  $P_{-a-b}$ , respectively, are measurable quantities by means of the joint photodetections of  $D_A^+ & D_B^+$ ,  $D_A^- & D_B^+$ ,  $D_A^+ & D_B^-$ , and  $D_A^- & D_B^-$ . A typical experimental observation of  $E(\theta_A, \theta_B)$  from a Bell state is shown in ■ Fig. 16.12. Bell's inequality violation is expected from this measurement.

### 16.3 Scully's Quantum Eraser

Quantum eraser, proposed by Scully and Drühl in 1982 [9], is another thought experiment challenge the “basic mystery” of quantum mechanics: wave-particle duality. So far, several quantum eraser experiments have been demonstrated with interesting results supporting the ideas of Scully and Drühl [10, 11, 34, 35].

A double-slit type quantum eraser experiment, closing to the original Scully–Drühl thought experiment of 1982, is illustrated in Fig. 16.13. A pair of entangled photons, photon 1 and photon 2, is excited by a weak laser pulse either from atom A, which is located in slit A, or from atom B, which is located in slit B. Photon 1, propagates to the right, is registered by detector  $D_0$ , which can be scanned by a step motor along its  $x_0$ -axis for the examination of interference fringes. Photon 2, propagating to the left, is injected into a beamsplitter. If the pair is generated in atom A, photon 2 will follow the A path meeting BSA with 50 % chance of being reflected or transmitted. If the pair is generated in atom B, photon 2 will follow the B path meeting BSB with 50 % chance of being reflected or transmitted. In view of the 50 % chance of being transmitted by either BSA or BSB, photon 2 is detected by either detector  $D_3$  or  $D_4$ . The registration of  $D_3$  or  $D_4$  provides which-path information (path A or path B) on photon 2 and in turn provides which-path information for photon 1 because of the entanglement nature of the two-photon state generated by atomic cascade decay. Given a reflection at either BSA or BSB photon 2 will continue to follow its A or B path to meet another 50–50 beamsplitter BS and then be detected by either detectors  $D_1$  or  $D_2$ .

The experimental condition was arranged in such a way that no interference is observable in the single counting rate of  $D_0$ , i.e., the distance between A and B is large enough to be “distinguishable” for  $D_0$  to learn which-path information of photon 1. However, the “clicks” at  $D_1$  or  $D_2$  will erase the which-path information of photon 1 and help to restore the interference. On the other hand, the “clicks” at  $D_3$  or  $D_4$  record which-path information. Thus, no observable interference is expected with the help of these “clicks.” It is interesting to note that both the “erasure” and “recording” of the which-path information can be made as a “delayed choice”: the experiment is designed in such a way that  $L_0$ , the optical distance between atoms A, B and detector  $D_0$ , is much shorter than  $L_A$  ( $L_B$ ), which is the optical distance between atoms A, B and the beamsplitter BSA (BSB) where the “which-path” or “both-paths” “choice” is made randomly by photon 2. Thus, after the annihilation of photon 1 at  $D_0$ , photon 2 is still on its way to BSA (BSB), i.e., “which-path” or “both-paths” choice is “delayed” compared to the detection of

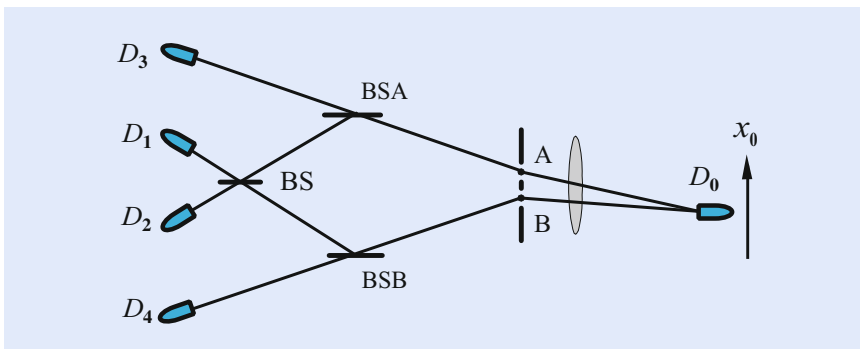


**Fig. 16.13** Quantum erasure: a thought experiment of Scully–Drühl. A pair of entangled photons is emitted from either atom A or atom B by atomic cascade decay. The experimental condition guarantees no interference fringes is observable in the single detector counting rate of  $D_0$ . The “clicks” at  $D_1$  or  $D_2$  erase the which-path information, thus helping to restore the interference even after the “click” of  $D_0$ . On the other hand, the “clicks” at  $D_3$  or  $D_4$  record which-slit information. Thus, no observable interference is expected with the help of these “clicks”

photon 1. After the annihilation of photon 1, we look at these “delayed” detection events of  $D_1$ ,  $D_2$ ,  $D_3$ , and  $D_4$  which have constant time delays,  $\tau_i \simeq (L_i - L_0)/c$ , relative to the triggering time of  $D_0$ .  $L_i$  is the optical distance between atoms A, B and detectors  $D_1$ ,  $D_2$ ,  $D_3$ , and  $D_4$ , respectively. It was predicted that the “joint-detection” counting rate  $R_{01}$  (joint-detection rate between  $D_0$  and  $D_1$ ) and  $R_{02}$  will show an interference pattern as a function of the position of  $D_0$  on its  $x$ -axis. This reflects the wave nature (both-path) of photon 1. However, no interference fringes will be observable in the joint detection counting events  $R_{03}$  and  $R_{04}$  when scanning detector  $D_0$  along its  $x$ -axis. This is as would be expected because we have now inferred the particle (which-path) property of photon 1. It is important to emphasize that all four joint detection rates  $R_{01}$ ,  $R_{02}$ ,  $R_{03}$ , and  $R_{04}$  are recorded at the same time during one scanning of  $D_0$ . That is, in the present experiment, we “see” both wave (interference) and which-path (particle-like) with the same measurement apparatus.

It should be mentioned that (1) the “choice” in this experiment is not actively switched by the experimentalist during the measurement. The “delayed choice” associated with either the wave or particle behavior of photon 1 is “randomly” made by photon 2. The experimentalist simply looks at which detector  $D_1$ ,  $D_2$ ,  $D_3$  or  $D_4$  is triggered by photon 2 to determine either wave or particle properties of photon 1 after the annihilation of photon 1; (2) the photo-detection event of photon 1 at  $D_0$  and the delayed choice event of photon 2 at BSA (BSB) are space-like separated events. The “coincidence” time window is chosen to be much shorter than the distance between  $D_0$  and BSA (BSB). Within the joint-detection time window, it is impossible to have the two events “communicating.”

### 16.3.1 Random Delayed Choice Quantum Eraser One

Kim et al. realized the above random delayed choice quantum eraser in 2000 [10]. The schematic diagram of the experimental setup of Kim et al. is shown in Fig. 16.14. Instead of atomic cascade decay, SPDC is used to prepare the entangled two-photon state.

In the experiment, a 351.1 nm Argon ion pump laser beam is divided by a double-slit and directed onto a type-II phase matching nonlinear crystal BBO at regions A and B. A pair of 702.2 nm orthogonally polarized signal-idler photon is

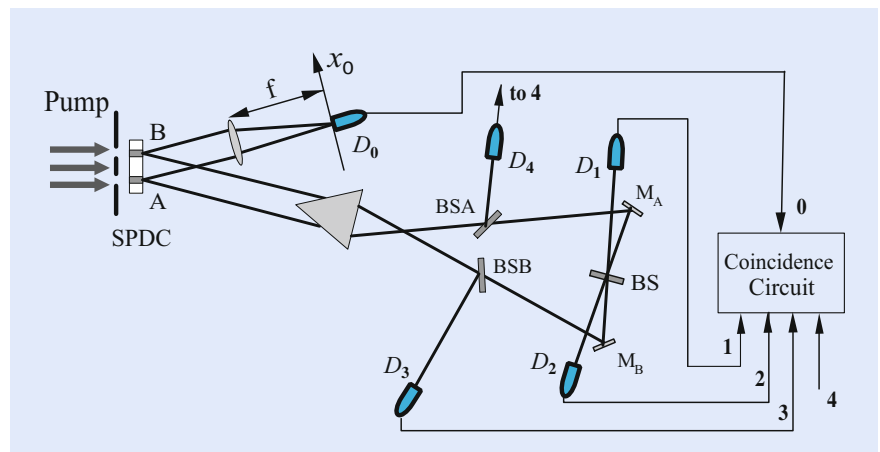
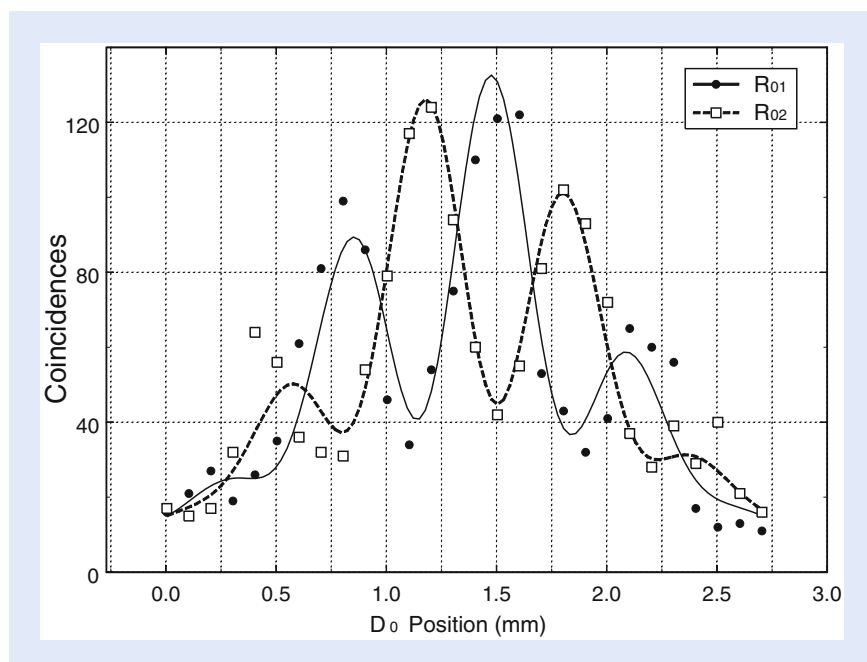


Fig. 16.14 Delayed choice quantum eraser: Schematic of an actual experimental setup of Kim et al. Pump laser beam is divided by a double-slit and makes two regions A and B inside the SPDC crystal. A pair of signal-idler photons is generated either from the A or B region. The “delayed choice” to observe either wave or particle behavior of the signal photon is made randomly by the idler photon about 7.7 ns after the detection of the signal photon

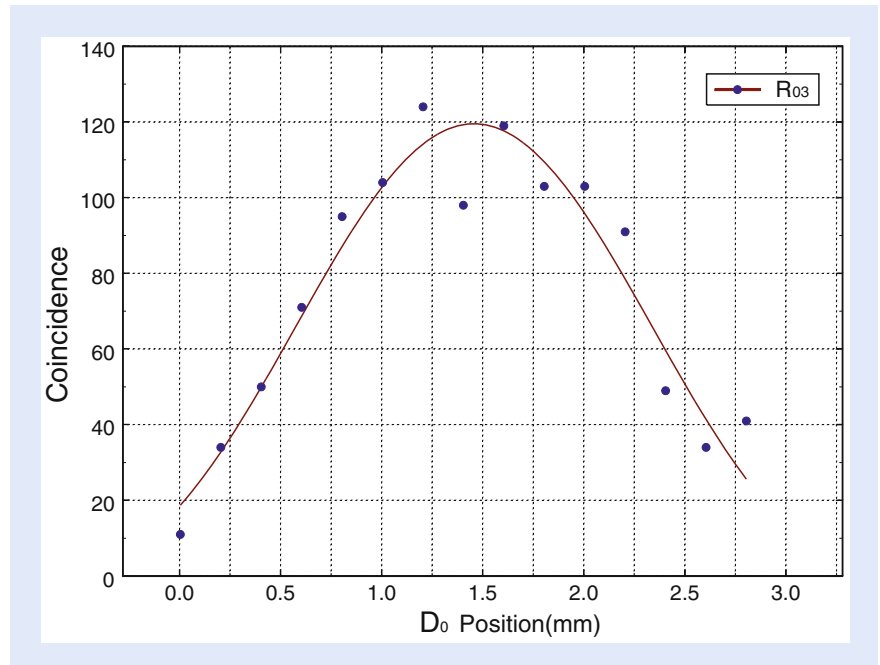
generated either from region A or region B. The width of the region is about  $a = 0.3$  mm and the distance between the center of A and B is about  $d = 0.7$  mm. A Glen-Thompson prism is used to split the orthogonally polarized signal and idler. The signal photon (photon 1, coming either from A or B) propagates through lens  $LS$  to detector  $D_0$ , which is placed on the Fourier transform plane of the lens. The use of lens  $LS$  is to achieve the “far field” condition, but still keep a short distance between the slit and the detector  $D_0$ . Detector  $D_0$  can be scanned along its  $x$ -axis by a step motor for the observation of interference fringes. The idler photon (photon 2) is sent to an interferometer with equal-path optical arms. The interferometer includes a prism  $PS$ , two 50–50 beamsplitters  $BSA$ ,  $BSB$ , two reflecting mirrors  $M_A$ ,  $M_B$ , and a 50–50 beamsplitter  $BS$ . Detectors  $D_1$  and  $D_2$  are placed at the two output ports of the  $BS$ , respectively, for erasing the which-path information. The triggering of detectors  $D_3$  and  $D_4$  provides which-path information for the idler (photon 2) and, in turn, which-path information for the signal (photon 1). The detectors are fast avalanche photodiodes with less than 1 ns rise time and about 100 ps jitter. A constant fractional discriminator is used with each of the detectors to register a single photon whenever the leading edge of the detector output pulse is above the threshold. Coincidences between  $D_0$  and  $D_j$  ( $j = 1, 2, 3, 4$ ) are recorded, yielding the joint detection counting rates  $R_{01}$ ,  $R_{02}$ ,  $R_{03}$ , and  $R_{04}$ .

In the experiment, the optical delay ( $L_{A, B} - L_0$ ) is chosen to be  $\simeq 2.3$  m, where  $L_0$  is the optical distance between the output surface of  $BBO$  and detector  $D_0$ , and  $L_A$  ( $L_B$ ) is the optical distance between the output surface of the  $BBO$  and the beamsplitter  $BSA$  ( $BSB$ ). This means that any information (which-path or both-path) one can infer from photon 2 must be at least 7.7 ns later than the registration of photon 1. Compared to the 1 ns response time of the detectors, 2.3 m delay is thus enough for “delayed erasure.” Although there is an arbitrariness about when a photon is detected, it is safe to say that the “choice” of photon 2 is delayed with respect to the detection of photon 1 at  $D_0$  since the entangled photon pair is created simultaneously.

■ Figure 16.15 reports the joint detection rates  $R_{01}$  and  $R_{02}$ , indicating the regaining of standard Young’s double-slit interference pattern. An expected  $\pi$



■ Fig. 16.15 Joint detection rates  $R_{01}$  and  $R_{02}$  against the  $x$  coordinates of detector  $D_0$ . Standard Young’s double-slit interference patterns are observed. Note the  $\pi$  phase shift between  $R_{01}$  and  $R_{02}$ . The solid line and the dashed line are theoretical fits to the data



■ **Fig. 16.16** Joint detection counting rate of  $R_{03}$ . Absence of interference is clearly demonstrated. The *solid line* is a sinc-function fit

phase shift between the two interference patterns is clearly shown in the measurement. The single detector counting rates of  $D_0$  and  $D_1$  are recorded simultaneously. Although interference is observed in the joint detection counting rate, there is no significant modulation in any of the single detector counting rate during the scanning of  $D_0$ .  $R_0$  is a constant during the scanning of  $D_0$ . The absence of interference in the single detector counting rate of  $D_0$  is simply because the separation between slits A and slit B is much greater than the coherence length of the single field.

■ Figure 16.16 reports a typical  $R_{03}$  ( $R_{04}$ ), joint detection counting rate between  $D_0$  and “which-path detector”  $D_3$  ( $D_4$ ). An absence of interference is clearly demonstrated. The fitting curve of the experimental data indicates a sinc-function like envelope of the standard Young’s double slit interference-diffraction pattern. Two features should bring to our attention that (1) there is no observable interference modulation as expected, and (2) the curve is different from the constant single detector counting rate of  $D_0$ .

The experimental result is surprising from a classical point of view. The result, however, is easily explained in the contents of quantum theory. In this experiment, there are two kinds of very different interference phenomena: single-photon interference and two-photon interference. As we have discussed earlier, single-photon interference is the result of the superposition between single-photon amplitudes, and two-photon interference is the results of the superposition between two-photon amplitudes. Quantum mechanically, single-photon amplitude and two-photon amplitude represent very different measurements and, thus, very different physics.

In this regard, we analyze the experiment by answering the following questions:

- (1) Why is there no observable interference in the single-detector counting rate of  $D_0$ ?

This question belongs to single-photon interferometry. The absence of interference in single-detector counting rate of  $D_0$  is very simple: the separation

between slit A and slit B is much greater than the coherence length of the signal field.

- (2) Why is there observable interference in the joint detection counting rate of  $D_{01}$  and  $D_{02}$ ?

This question belongs to two-photon interferometry. Two-photon interference is very different from single-photon interference. Two-photon interference involves the addition of different yet indistinguishable two-photon amplitudes. The coincidence counting rate  $R_{01}$ , again, is proportional to the probability  $P_{01}$  of joint detecting the signal-idler pair by detectors  $D_0$  and  $D_1$ ,

$$R_{01} \propto P_{01} = \langle \Psi | E_0^{(-)} E_1^{(-)} E_1^{(+)} E_0^{(+)} | \Psi \rangle = |\langle 0 | E_1^{(+)} E_0^{(+)} | \Psi \rangle|^2. \quad (16.68)$$

To simplify the mathematics, we use the following “two-mode” expression for the state, bearing in mind that the transverse momentum  $\delta$ -function will be taken into account.

$$|\Psi\rangle = \varepsilon [a_s^\dagger a_i^\dagger e^{i\varphi_A} + b_s^\dagger b_i^\dagger e^{i\varphi_B}] |0\rangle$$

where  $\varepsilon$  is a normalization constant that is proportional to the pump field and the nonlinearity of the SPDC crystal,  $\varphi_A$  and  $\varphi_B$  are the phases of the pump field at A and B, and  $a_j^\dagger$  ( $b_j^\dagger$ ),  $j = s, i$ , are the photon creation operators for the lower (upper) mode in [Fig. 16.14](#).

In Eq. (16.68), the fields at the detectors  $D_0$  and  $D_1$  are given by

$$\begin{aligned} E_0^{(+)} &= a_s e^{ikr_{A0}} + b_s e^{ikr_{B0}} \\ E_1^{(+)} &= a_i e^{ikr_{A1}} + b_i e^{ikr_{B1}} \end{aligned} \quad (16.69)$$

where  $r_{Aj}$  ( $r_{Bj}$ ),  $j = 0, 1$  are the optical path lengths from region A (B) to the  $j$ th detector. Substituting the biphoton state and the field operators into Eq. (16.68),

$$\begin{aligned} R_{01} &\propto |e^{i(kr_A + \varphi_A)} + e^{i(kr_B + \varphi_B)}|^2 = |\Psi_A + \Psi_B|^2 \\ &= 1 + \cos[k(r_A - r_B)] \simeq \cos^2(x_0 \pi d / \lambda z_0) \end{aligned} \quad (16.70)$$

where  $r_A = r_{A0} + r_{A1}$ ,  $r_B = r_{B0} + r_{B1}$ ;  $\Psi_A$  and  $\Psi_B$  are the two-photon effective wave functions of path A and path B, representing the two different yet indistinguishable probability amplitudes to produce a joint photodetection event of  $D_0$  and  $D_1$ , indicating a two-photon interference. In Dirac’s language: a signal-idler photon pair interferes with the pair itself.

To calculate the diffraction effect of a single-slit, again, we need an integral of the effective two-photon wavefunction over the slit width (the superposition of infinite number of probability amplitudes results in a click-click joint detection event):

$$R_{01} \propto \left| \int_{-a/2}^{a/2} dx_{AB} e^{-ik r(x_0, x_{AB})} \right|^2 \cong \text{sinc}^2(x_0 \pi a / \lambda z_0) \quad (16.71)$$

where  $r(x_0, x_{AB})$  is the distance between points  $x_0$  and  $x_{AB}$ ,  $x_{AB}$  belongs to the slit’s plane, and the far-field condition is applied.

Repeating the above calculations, the combined interference-diffraction joint detection counting rate for the double-slit case is given by

$$R_{01} \propto \text{sinc}^2(x_0\pi a/\lambda z_0) \cos^2(x_0\pi d/\lambda z_0). \quad (16.72)$$

If the finite size of the detectors is taken into account, the interference visibility will be reduced.

- (3) Why is there no observable interference in the joint detection counting rate of  $R_{03}$  and  $R_{04}$ ?

This question belongs to two-photon interferometry. From the view of two-photon physics, the absence of interference in the joint detection counting rate of  $R_{03}$  and  $R_{04}$  is obvious: only one two-photon amplitude contributes to the joint detection events.

### 16.3.2 Random Delayed Choice Quantum Eraser Two

Now we ask, again, what would happen if we replace the entangled photons with a randomly paired photons, or wavepackets, in thermal state? Can a randomly paired photons in thermal state erase the which-path information? The answer is, again, positive. A random delayed choice quantum eraser using randomly paired photons in thermal state has been demonstrated by Peng et al. recently [11].

The experiment setup of Peng et al. is schematically illustrated in Fig. 16.17. The experimental setup is almost the same as that of the experiment of Kim et al. of 2000, except the photon source and the coincidence measurement: the randomly paired photons, or wavepackets are created from a standard pseudo-thermal source and the pulse this quantum eraser measures the photon-number fluctuation-correlation of thermal light. Thermal light has a peculiar “spatial coherence” property: the fluctuation of the measured photon-numbers, or intensities, correlated within its spatial coherence area only. When the measurements are beyond its coherence area, the photon-numbers fluctuation correlation vanish:

$$\langle \Delta n_A \Delta n_B \rangle \propto |G^{(1)}(\vec{\rho}_A, \vec{\rho}_B)|^2, \quad (16.73)$$

where  $\Delta n_j$ ,  $j = A, B$ , is the photon-number fluctuation at  $(\vec{\rho}_j, t_j)$  of the double-slit plane,  $G^{(1)}(\vec{\rho}_A, \vec{\rho}_B)$  is the first-order spatial coherence function of the thermal field. The spatial coherence of thermal light guarantees the photon-numbers fluctuate correlatively only when  $|\vec{\rho}_A - \vec{\rho}_B| < l_c$ , where  $l_c$  is the spatial coherence length. In this experiment, we choose  $|\vec{\rho}_A - \vec{\rho}_B| \gg l_c$ . Under this condition, we have achieved  $\langle \Delta n_A \Delta n_{A'} \rangle \neq 0$ ,  $\langle \Delta n_B \Delta n_{B'} \rangle \neq 0$  but  $\langle \Delta n_A \Delta n_B \rangle = 0$ . Note, again, here  $(\vec{\rho}_j)$  is on the double-slit plane, see Fig. 16.17. This peculiar property of thermal light together with the photon-number fluctuation-correlation measurement between  $D_0$  and  $D_3$  (or  $D_4$ ) provides the which-path information. It is interesting, the which-slit information is erasable in the fluctuation-correlation measurement between  $D_0$  and  $D_1$  (or  $D_2$ ).

The experimental setup in Fig. 16.17 can be divided into four parts: a thermal light source, a Young’s double-slit interferometer, a Mach–Zehnder-like interferometer, and a photon-number fluctuation-correlation measurement circuit. (1) The light source is a standard pseudo-thermal source [29] which consists of a He-Ne laser beam ( $\sim 2$  mm diameter) and a rotating ground glass (GG). Within the  $\sim 2$  mm diameter spot, the ground glass contains millions of tiny diffusers. A large number of randomly distributed sub-fields, or wavepacket, are scattered from millions of randomly distributed tiny diffusers with random phases. The pseudothermal field then passes a double-slit which is about 25 cm away from



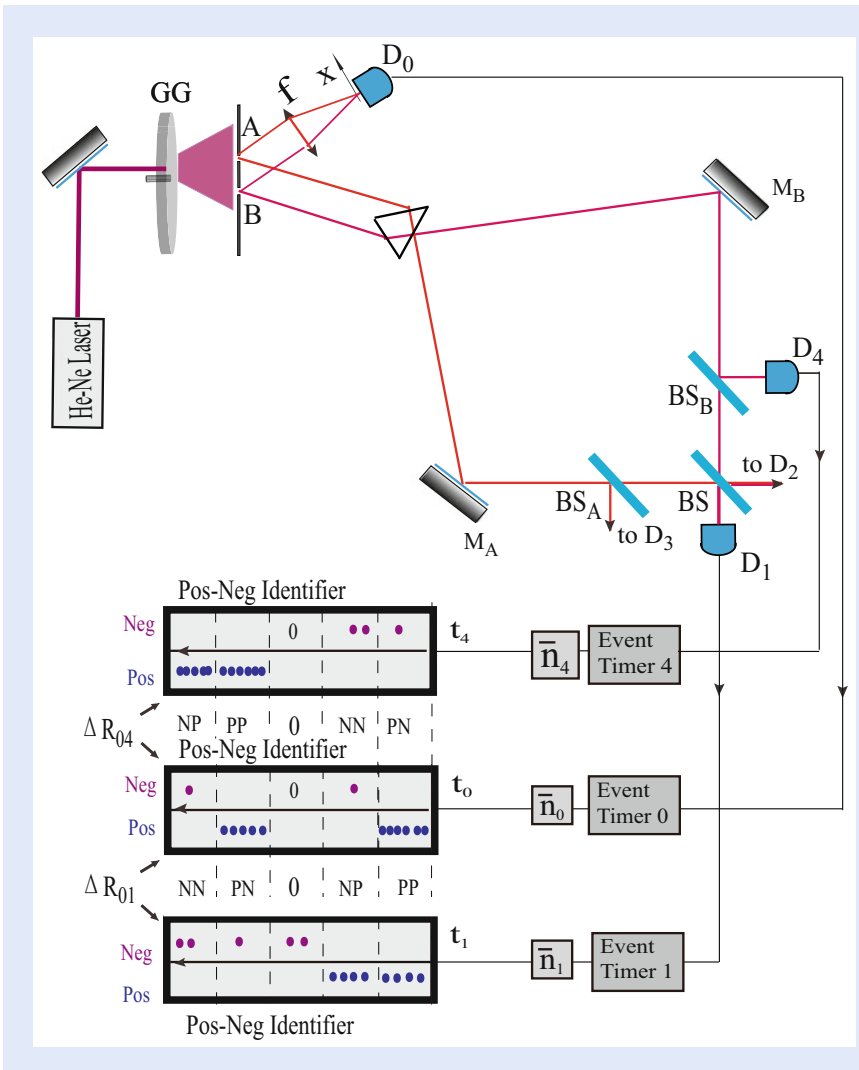


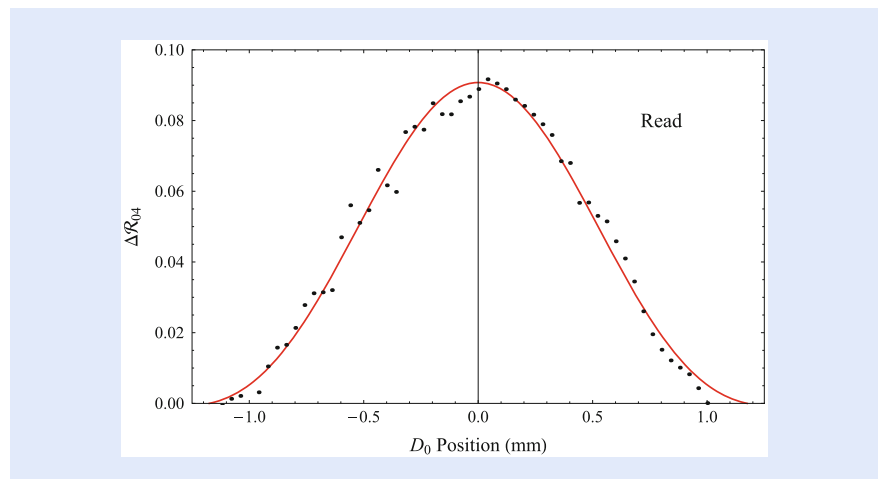
**Fig. 16.17** Schematic of a random delayed choice quantum eraser. The He-Ne laser beam spot on the rotating ground glass has a diameter of  $\sim 2$  mm. A double-slit, with slit-width  $150 \mu\text{m}$  and slit-separation  $0.7$  mm, is placed  $\sim 25$  cm away from the GG. The spatial coherence length of the pseudo-thermal field on the double-slit plane is calculated from Eq. (16.73),  $l_c = \lambda/\Delta\theta \sim 160 \mu\text{m}$ , which guarantees the two fields  $E_A$  and  $E_B$  are spatially incoherent. Under this experimental condition, the photon number fluctuates correlatively only within slit A or slit B. All beamsplitters are non-polarizing and 50/50. The two fields from the two slits may propagate to detector  $D_0$  which is transversely scanned on the focal plan of lens  $f$  for observing the interference pattern of the double-slit interferometer; and may also pass a long a Mach-Zehnder-like interferometer and finally reach at  $D_1$  or  $D_4$  ( $D_2$  or  $D_3$ ). A positive-negative fluctuation-correlation protocol is followed to evaluate the photon-number fluctuation-correlations from the coincidences between  $D_0$ - $D_1$  and  $D_0$ - $D_4$  (or  $D_0$ - $D_2$  and  $D_0$ - $D_3$ )

the GG. The spatial coherence length of the pseudo-thermal field on the double slit plane is calculated from Eq. (16.73),  $l_c = \lambda/\Delta\theta \sim 160 \mu\text{m}$ , which guarantees the spatial incoherence of the two fields  $E_A$  and  $E_B$  that passing through slit A and slit B, respectively. Under this experimental condition, the photon-numbers fluctuate correlatively only within slit-A or slit-B. We therefore learn the which-slit information in a photon number-fluctuation correlation measurement. (2) The double-slit has a slit-width  $150 \mu\text{m}$ , and a slit-separation  $0.7$  mm (distance between the center of two slits). A lens,  $f$ , is placed following the double-slit. On the focal-plane of the lens a scannable point-like photodetector  $D_0$  is used to learn

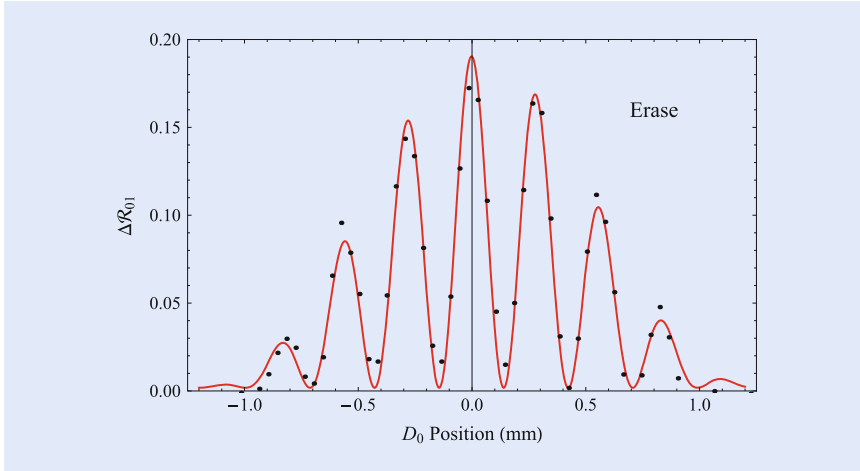
the which-slit information or to observe the Young's double-slit interference pattern. (3) The Mach-Zehnder-like interferometer and the photodetectors  $D_1$ ,  $D_2$  are used to "erase" the which-slit information. Simultaneously, the joint-detection between  $D_0$  and  $D_3$  or  $D_4$  is used to "learn" the which-slit information. All five photodetectors are photon-counting detectors working at single-photon level. The Mach-Zehnder-like interferometer has three beamsplitters,  $BS$ ,  $BS_A$ , and  $BS_B$ , all of them are 50/50 non-polarizing beamsplitters. Moreover, the detectors are fast avalanche photodiodes with rise time less than 1 ns, and the path delay between  $BS_A$  or  $BS_B$ , and  $D_0$  is  $\approx 1.5$  m which ensure that, at each joint-detection measurement, when a photon chooses to be reflected (read which-way) or transmitted (erase which-way) at  $BS_A$  or  $BS_B$ , it is already 5 ns later than the annihilation of its partner at  $D_0$ . Comparing the 1 ns rise time, we are sure this is a "delayed choice" made by that photon. (4) The photon-number fluctuation-correlation circuit consists of five synchronized "event-timers" which record the registration times of  $D_0$ ,  $D_1$ ,  $D_2$ ,  $D_3$ , and  $D_4$ . A positive-negative fluctuation identifier follows each event-timer to distinguish "positive-fluctuation"  $\Delta n^+$ , from "negative-fluctuation"  $\Delta n^-$ , for each photodetector within each coincidence time window. The photon-number fluctuation-correlations of  $D_0$ - $D_1$ :  $\Delta R_{01} = \langle \Delta n_0 \Delta n_1 \rangle$  and  $D_0$ - $D_4$ :  $\Delta R_{04} = \langle \Delta n_0 \Delta n_4 \rangle$  are calculated, accordingly and respectively, based on their measured positive-negative fluctuations. The detailed description of the photon-number fluctuation-correlation circuit can be found in [30].

The experimental observation of  $\Delta R_{04}$  is reported in ■ Fig. 16.18. The data excludes any possible existing interferences. This measurement means the coincidences that contributed to  $\Delta R_{04}$  must have passed through slit B. ■ Figure 16.19 reports a typical experimental result of  $\Delta R_{01}$ : a typical double-slit interference-diffraction pattern. The 100 % visibility of the sinusoidal modulation indicates complete erasure of the which-slit information.

Assuming a random pair of sub-fields at single-photon level, such as the  $m$ th and  $n$ th wavepackets, is scattered from the  $m$ th and the  $n$ th sub-sources located at transverse coordinates  $\vec{\rho}_{0m}$  and  $\vec{\rho}_{0n}$  of the ground glass and fall into the coincidence time windows of  $D_0$ - $D_1$  and  $D_0$ - $D_4$ , the  $m$ th wavepacket may propagate to the double-slit interferometer and the  $n$ th wavepacket may pass through the Mach-Zehnder, or vice versa. Under the experimental condition of spatial incoherence between  $E_A$  and  $E_B$ , the which-slit information is learned from the photon-number



■ Fig. 16.18 The measured  $\Delta R_{04}$  by scanning  $D_0$  on the observation plane of the Young's double-slit interferometer. The black dots are experimental data, the red line is the theoretical fitting with Eq. (16.81)



■ **Fig. 16.19** The measured  $\Delta R_{01}$  as a function of the transverse coordinate of  $D_0$ . The black dots are experimental data, the red line is the theoretical fitting with Eq. (16.82)

fluctuation-correlation measurements  $\Delta R_{04} = \langle \Delta n_0 \Delta n_4 \rangle = \langle \Delta n_{B0} \Delta n_{B4} \rangle$  of  $D_0$ - $D_4$ , and no interference is observable by scanning  $D_0$ . It is interesting that the which-slit information are erasable in the photon-number fluctuation-correlation measurements of  $\Delta R_{01} = \langle \Delta n_0 \Delta n_1 \rangle$  of  $D_0$ - $D_1$ , resulting in a reappeared interference pattern as a function of the scanning coordinate of  $D_0$ .

The field operator at detector  $D_0$  can be written in the following form in terms of the subfields:

$$\begin{aligned}
 \hat{E}^{(+)}(\mathbf{r}_0, t_0) &= \hat{E}_A^{(+)}(\mathbf{r}_0, t_0) + \hat{E}_B^{(+)}(\mathbf{r}_0, t_0) \\
 &= \sum_m \left[ \hat{E}_{mA}^{(+)}(\mathbf{r}_0, t_0) + \hat{E}_{mB}^{(+)}(\mathbf{r}_0, t_0) \right] \\
 &= \sum_m \int d\mathbf{k} \hat{a}_m(\mathbf{k}) [g_m(\mathbf{k}; \mathbf{r}_A, t_A) g_A(\mathbf{k}; \mathbf{r}_0, t_0) \\
 &\quad + g_m(\mathbf{k}; \mathbf{r}_B, t_B) g_B(\mathbf{k}; \mathbf{r}_0, t_0)].
 \end{aligned} \tag{16.74}$$

where  $g_m(\mathbf{k}; \mathbf{r}_s, t_s)$  is a Green's function which propagates the  $m$ th subfield from the  $m$ th sub-source to the  $s$ th slit ( $s = A, B$ ).  $g_s(\mathbf{k}; \mathbf{r}_0, t_0)$  is another Green's function that propagates the field from the  $s$ th slit to detector  $D_0$ . It is easy to notice that, although there are two ways a photon can be detected at  $D_0$ , due to the first order incoherence of  $E_A$  and  $E_B$ , there should be no interference at the detection plane.

$D_4$  ( $D_3$ ) in the experiment can only receive photons from slit B (slit A), so the field operator is then:

$$\begin{aligned}
 \hat{E}^{(+)}(\mathbf{r}_4, t_4) &= \sum_m \hat{E}_{mB}^{(+)}(\mathbf{r}_4, t_4) \\
 &= \sum_m \int d\mathbf{k} \hat{a}_m(\mathbf{k}) g_m(\mathbf{k}; \mathbf{r}_B, t_B) g_B(\mathbf{k}; \mathbf{r}_4, t_4).
 \end{aligned} \tag{16.75}$$

The detector  $D_1$  ( $D_3$ ), however, can receive photons from both slit A and slit B through the Mach-Zehnder-like interferometer, so the field operator has two terms:

$$\begin{aligned}
\hat{E}^{(+)}(\mathbf{r}_1, t_1) &= \sum_m \left[ \hat{E}_{mA}^{(+)}(\mathbf{r}_1, t_1) + \hat{E}_{mB}^{(+)}(\mathbf{r}_1, t_1) \right] \\
&= \sum_m \int d\mathbf{k} \hat{a}_m(\mathbf{k}) [g_m(\mathbf{k}; \mathbf{r}_A, t_A) g_A(\mathbf{k}; \mathbf{r}_1, t_1) \\
&\quad + g_m(\mathbf{k}; \mathbf{r}_B, t_B) g_B(\mathbf{k}; \mathbf{r}_1, t_1)].
\end{aligned} \tag{16.76}$$

Based on the state of Eq. (16.32) and the field operators of Eqs. (16.74–16.76), we apply the Glauber-Scully theory [25, 36] to calculate the photon-number fluctuation-correlation or the second-order coherence function  $G^{(2)}(\mathbf{r}_0, t_0; \mathbf{r}_\alpha, t_\alpha)$  from the coincidence measurement of  $D_0$  and  $D_\alpha$  ( $\alpha = 1, 2, 3, 4$ ):

$$\begin{aligned}
G^{(2)}(\mathbf{r}_0, t_0; \mathbf{r}_\alpha, t_\alpha) &= \langle \langle \Psi | E^{(-)}(\mathbf{r}_0, t_0) E^{(-)}(\mathbf{r}_\alpha, t_\alpha) E^{(+)}(\mathbf{r}_\alpha, t_\alpha) E^{(+)}(\mathbf{r}_0, t_0) | \Psi \rangle \rangle_{Es} \\
&= \left\langle \left\langle \Psi \left| \sum_m E_m^{(-)}(\mathbf{r}_0, t_0) \sum_n E_n^{(-)}(\mathbf{r}_\alpha, t_\alpha) \sum_q E_q^{(+)}(\mathbf{r}_\alpha, t_\alpha) \sum_p E_p^{(+)}(\mathbf{r}_0, t_0) \right| \Psi \right\rangle \right\rangle_{Es} \\
&= \sum_m \psi_m^*(\mathbf{r}_0, t_0) \psi_m(\mathbf{r}_0, t_0) \sum_n \psi_n^*(\mathbf{r}_\alpha, t_\alpha) \psi_n(\mathbf{r}_\alpha, t_\alpha) \\
&\quad + \sum_{m,n} \psi_m^*(\mathbf{r}_0, t_0) \psi_n(\mathbf{r}_0, t_0) \psi_n^*(\mathbf{r}_\alpha, t_\alpha) \psi_m(\mathbf{r}_\alpha, t_\alpha) \\
&= \langle n_0 \rangle \langle n_\alpha \rangle + \langle \Delta n_0 \Delta n_\alpha \rangle.
\end{aligned} \tag{16.77}$$

Here  $\psi_m(\mathbf{r}_\alpha, t_\alpha)$  is the effective wavefunction of the  $m$ th subfield at  $(\mathbf{r}_\alpha, t_\alpha)$ . In the case of  $\alpha = 1, 2$

$$\begin{aligned}
\psi_m(\mathbf{r}_\alpha, t_\alpha) &= \psi_{mA\alpha} + \psi_{mB\alpha} \\
&= \int d\mathbf{k} \alpha_m(\mathbf{k}) [g_m(\mathbf{k}; \mathbf{r}_A, t_A) g_A(\mathbf{k}; \mathbf{r}_\alpha, t_\alpha) + g_m(\mathbf{k}; \mathbf{r}_B, t_B) g_B(\mathbf{k}; \mathbf{r}_\alpha, t_\alpha)].
\end{aligned} \tag{16.78}$$

This shows that the measured effective wavefunction  $\psi_m(\mathbf{r}_\alpha, t_\alpha)$  is the result of a superposition between two alternative amplitudes in terms of path-A and path-B,  $\psi_{m\alpha} = \psi_{mA\alpha} + \psi_{mB\alpha}$ . When  $\alpha = 4$  (or  $\alpha = 3$ ), the effective wavefunction has only one amplitude

$$\psi_m(\mathbf{r}_4, t_4) = \psi_{mB4} = \int d\mathbf{k} \alpha_m(\mathbf{k}) g_m(\mathbf{k}; \mathbf{r}_B, t_B) g_B(\mathbf{k}; \mathbf{r}_4, t_4). \tag{16.79}$$

From Eq. (16.77) and the measurement circuit in Fig. 16.17, it is easy to find that what we measure in this experiment is the photon-number fluctuation-correlation:

$$\langle \Delta n_0 \Delta n_\alpha \rangle = \sum_{m,n} \psi_m^*(\mathbf{r}_0, t_0) \psi_n(\mathbf{r}_0, t_0) \psi_n^*(\mathbf{r}_\alpha, t_\alpha) \psi_m(\mathbf{r}_\alpha, t_\alpha). \tag{16.80}$$

We thus obtain

$$\Delta R_{04} \propto \langle \Delta n_0 \Delta n_4 \rangle = \sum_{n \neq m} \psi_{mB0}^* \psi_{nB0} \psi_{nB4}^* \psi_{mB4} \propto \text{sinc}^2(x\pi a / \lambda f), \tag{16.81}$$

indicating a diffraction pattern which agrees with the experimental observation of Fig. 16.18.

In the case of  $\alpha = 1, 2$ , we obtain

$$\begin{aligned} \Delta R_{01} &\propto \langle \Delta n_0 \Delta n_1 \rangle \\ &\propto \sum_{n \neq m} [\psi_{mA0}^* \psi_{nA0} \psi_{nA1}^* \psi_{mA1} + \psi_{mB0}^* \psi_{nB0} \psi_{nB1}^* \psi_{mB1} \\ &\quad + \psi_{mA0}^* \psi_{nB0} \psi_{nB1}^* \psi_{mA1} + \psi_{mB0}^* \psi_{nA0} \psi_{nA1}^* \psi_{mB1}] \\ &\propto \text{sinc}^2(x\pi a/\lambda f) \cos^2(x\pi d/\lambda f), \end{aligned} \quad (16.82)$$

which agrees with the experimental observation in [Fig. 16.19](#).

## 16.4 Popper's Experiment

Popper's original thought experiment is schematically shown in [Fig. 16.20](#) [12]. A point source S, positronium as Popper suggested, is placed at the center of the experimental arrangement from which entangled pair of particle 1 and particle 2 are emitted in opposite directions along the respective positive and negative  $x$ -axes towards two screens A and B. There are slits on both screens parallel to the  $y$ -axis and the slits may be adjusted by varying their widths  $\Delta y$ . Beyond the slits on each side stand an array of Geiger counters for the joint measurement of the particle pairs as shown in the figure. The entangled pair could be emitted to any direction in  $4\pi$  solid angles from the point source. However, if particle 1 is detected in a certain direction, particle 2 is then known to be in the opposite direction due to the momentum conservation of the quanta pair.

First, let us imagine the case in which slits A and B are both adjusted very narrowly. In this circumstance, particle 1 and particle 2 experience diffraction at slit A and slit B, respectively, and exhibit greater  $\Delta p_y$  for smaller  $\Delta y$  of the slits.

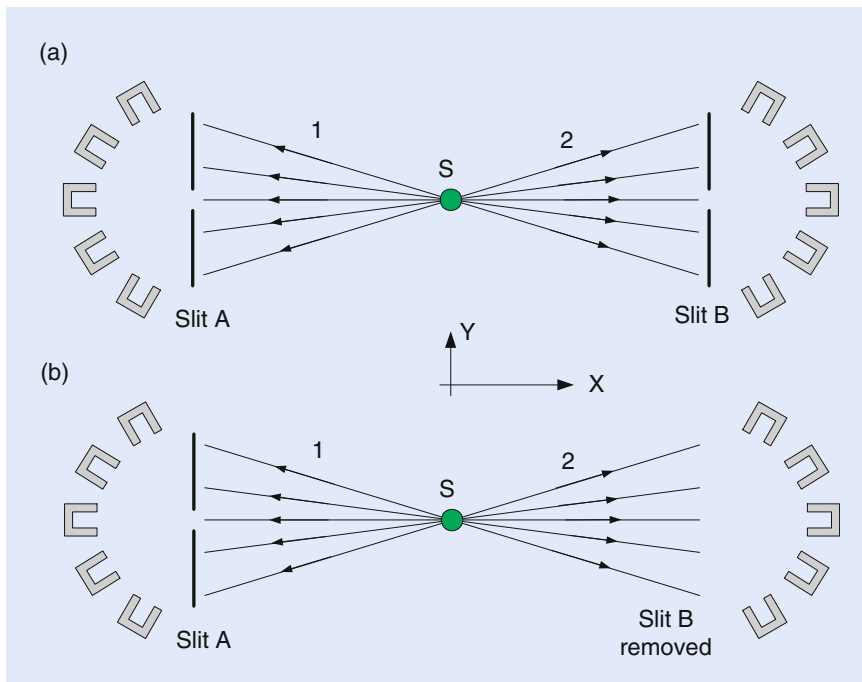


**Fig. 16.20** Popper's thought experiment. An entangled pair of particles are emitted from a point source with momentum conservation. A narrow slit on screen A is placed in the path of particle 1 to provide the precise knowledge of its position on the  $y$ -axis and this also determines the precise  $y$ -position of its twin, particle 2, on screen B. **(a)** Slits A and B are both adjusted very narrowly. **(b)** Slit A is kept very narrow and slit B is left wide open

There seems to be no disagreement in this situation between Copenhagen and Popper.

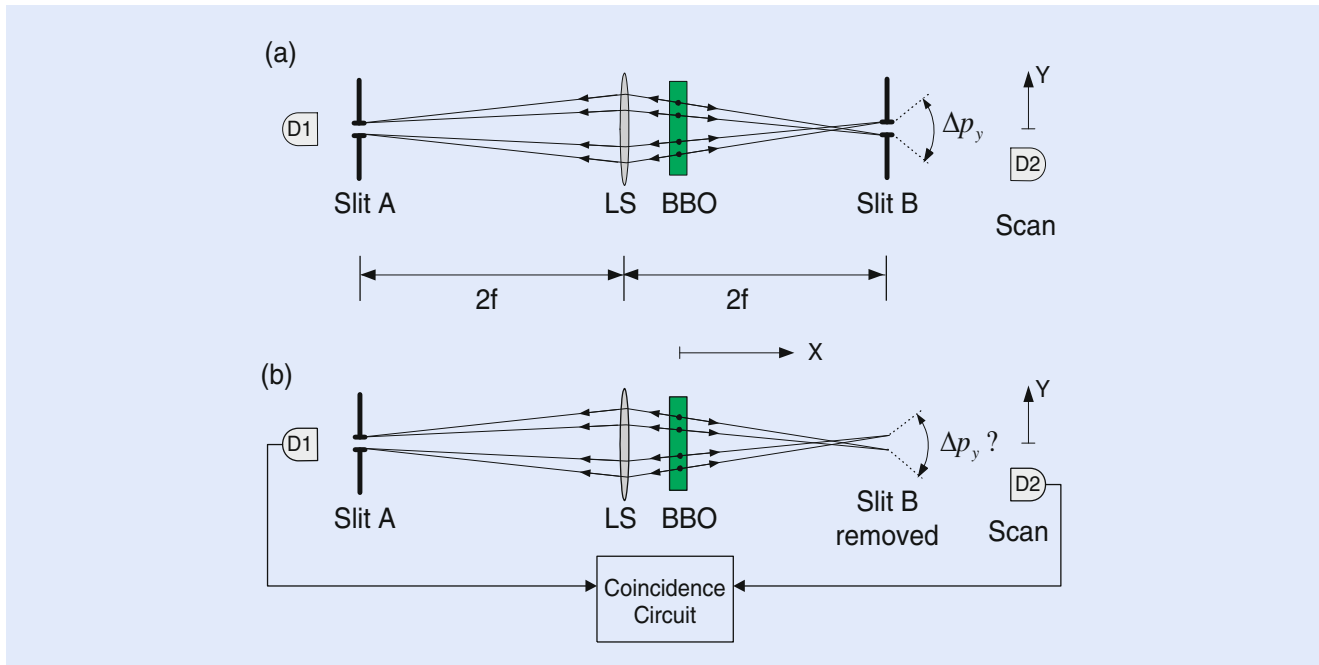
Next, suppose we keep slit A very narrow and leave slit B wide open. The main purpose of the narrow slit A is to provide the precise knowledge of the position  $y$  of particle 1 and this subsequently determines the precise position of its twin (particle 2) on side B through quantum entanglement. Now, Popper asks, in the absence of the physical interaction with an actual slit, does particle 2 experience a greater uncertainty in  $\Delta p_y$  due to the precise knowledge of its position? Based on his beliefs, Popper provides a straightforward prediction: *particle 2 must not experience a greater  $\Delta p_y$  unless a real physical narrow slit B is applied*. However, if Popper's conjecture is correct, this would imply the product of  $\Delta y$  and  $\Delta p_y$  of particle 2 could be smaller than  $h$  ( $\Delta y \Delta p_y < h$ ). This may pose a serious difficulty for Copenhagen and perhaps for many of us. On the other hand, if particle 2 going to the right does scatter like its twin, which has passed through slit A, while slit B is wide open, we are then confronted with an apparent *action-at-a-distance*!

The use of a *point source* in Popper's proposal has been criticized historically as the fundamental error Popper made. It is true that a point source can never produce a pair of entangled particles which preserves EPR correlation in momentum as Popper expected. However, notice that a *point source* is *not* a necessary requirement for Popper's experiment. What is required is a precise position-position EPR correlation: if the position of particle 1 is precisely known, the position of particle 2 is 100 % determined. Ghost imaging is a perfect tool to achieve this.

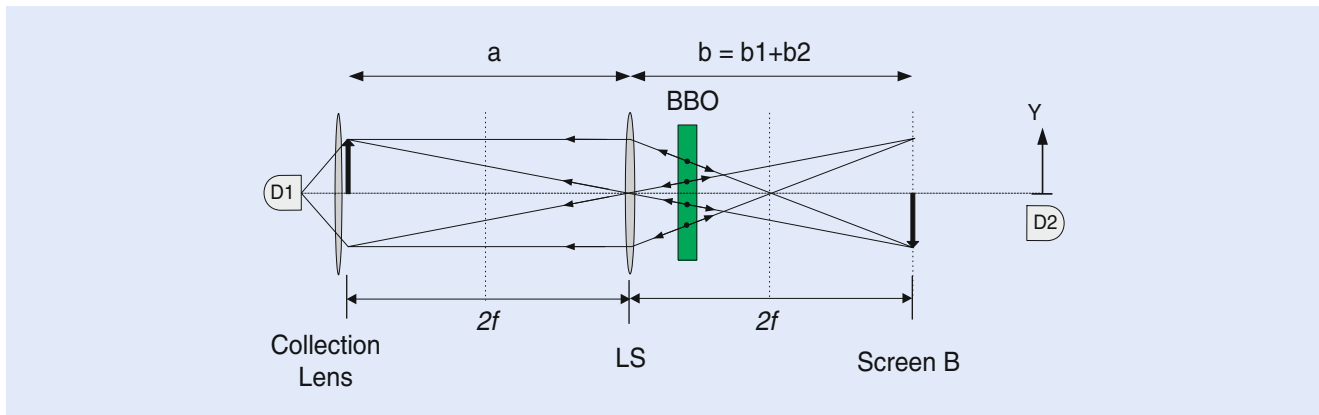
#### 16.4.1 Popper's Experiment One

In 1999, Popper's experiment was realized by Y.H. Kim et al. [13] with the help of biphoton ghost imaging [37]. ■ Figure 16.21 is a schematic diagram that is useful for comparison with the original Popper's thought experiment. It is easy to see that this is a typical ghost imaging experimental setup. An entangled photon pair is used to image slit A onto a distant image plane of "screen" B. In the setup,  $s_o$  is chosen to be twice the focal length of the imaging lens  $LS$ ,  $s_o = 2f$ . According to the Gaussian thin lens equation, an equal size "ghost" image of slit A appears on the two-photon image plane at  $s_i = 2f$ . The use of slit A provides a precise knowledge of the position of photon 1 on the  $y$ -axis and also determines the precise  $y$ -position of its twin, photon 2, on screen B by means of the biphoton ghost imaging. The experimental condition specified in Popper's experiment is then achieved: when slit A is adjusted to a certain narrow width and slit B is wide open, slit A provides precise knowledge about the position of photon 1 on the  $y$ -axis up to an accuracy  $\Delta y$  which equals the width of slit A, and the corresponding ghost image of pinhole A at screen B determines the precise position  $y$  of photon 2 to within the same accuracy  $\Delta y$ .  $\Delta p_y$  of photon 2 can be independently studied by measuring the width of its "diffraction pattern" at a certain distance from "screen" B. This is obtained by recording coincidences between detectors  $D_1$  and  $D_2$  while scanning detector  $D_2$  along its  $y$ -axis, which is behind screen B at a certain distance.

■ Figure 16.22 is a conceptual diagram to connect the modified Popper's experiment with biphoton ghost imaging. In this unfolded ghost imaging setup, we assume the entangled signal-idler photon pair holds a perfect EPR correlation in momentum with  $\delta(\mathbf{k}_s + \mathbf{k}_i) \sim 0$ , which can be easily realized in a large transverse sized SPDC. In this experiment, we have chosen  $s_o = s_i = 2f$ . Thus, an equal size ghost image of slit A is expected to appear on the image plane of screen B.

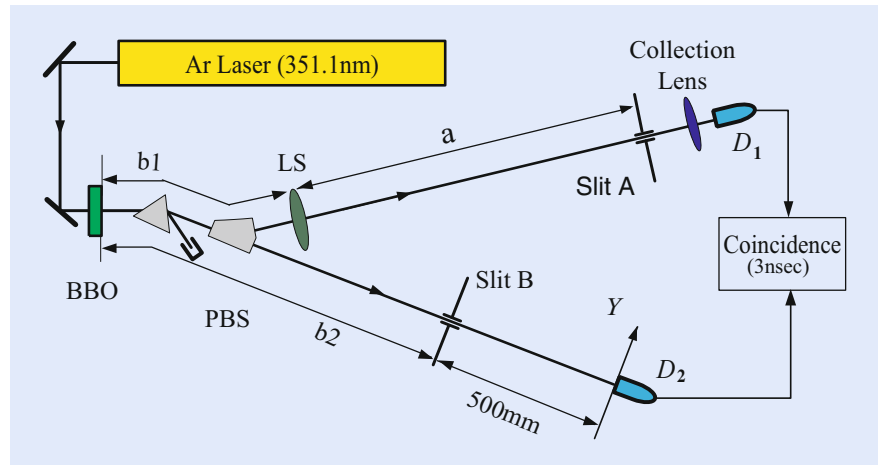


■ **Fig. 16.21** Modified version of Popper's experiment. An entangled photon pair is generated by SPDC. A lens and a narrow slit A are placed in the path of photon 1 to provide the precise knowledge of its position on the  $y$ -axis and also to determine the precise  $y$ -position of its twin, photon 2, on screen B by means of biphoton ghost imaging. Photon counting detectors  $D_1$  and  $D_2$  are used to scan in  $y$ -directions for joint detections. **(a)** Slits A and B are both adjusted very narrowly. **(b)** Slit A is kept very narrow and slit B is left wide open



■ **Fig. 16.22** An unfolded schematic of ghost imaging. We assume the entangled signal-idler photon pair holds a perfect momentum correlation  $\delta(\mathbf{k}_s + \mathbf{k}_i) \sim 0$ . The locations of the slit A, the imaging lens LS, and the ghost image must be governed by the Gaussian thin lens equation. In this experiment, we have chosen  $s_o = s_i = 2f$ . Thus, the ghost image of slit A is expected to be the same size as that of slit A

The detailed experimental setup is shown in ■ Fig. 16.23 with indications of the various distances. A CW Argon ion laser line of  $\lambda_p = 351.1$  nm is used to pump a 3 mm long beta barium borate (BBO) crystal for type-II SPDC to generate an orthogonally polarized signal-idler photon pair. The laser beam is about 3 mm in diameter with a diffraction limited divergence. It is important not to focus the pump beam so that the phase-matching condition,  $\mathbf{k}_s + \mathbf{k}_i = \mathbf{k}_p$ , is well reinforced in the SPDC process, where  $\mathbf{k}_j$  ( $j = s, i, p$ ) is the wavevectors of the signal ( $s$ ), idler ( $i$ ), and pump ( $p$ ) respectively. The collinear signal-idler beams, with  $\lambda_s = \lambda_i = 702.2$  nm =  $2\lambda_p$  are separated from the pump beam by a fused quartz dispersion prism, and then split by a polarization beam splitter PBS. The signal beam



■ **Fig. 16.23** Schematic of the experimental setup. The laser beam is about 3 mm in diameter. The “phase-matching condition” is well reinforced. Slit A (0.16 mm) is placed  $1000 \text{ mm} = 2f$  behind the converging lens, LS ( $f = 500 \text{ mm}$ ). The one-to-one ghost image (0.16 mm) of slit A is located at B. The optical distance from LS in the signal beam taken as back through PBS to the SPDC crystal ( $b_1 = 255 \text{ mm}$ ) and then along the idler beam to “screen B” ( $b_2 = 745 \text{ mm}$ ) is  $1000 \text{ mm} = 2f$  ( $b = b_1 + b_2$ )

(photon 1) passes through the converging lens LS with a 500 mm focal length and a 25 mm diameter. A 0.16 mm slit is placed at location A which is 1000 mm ( $s_o = 2f$ ) behind the lens LS. A short focal length lens is used with  $D_1$  for collecting all the signal beam that passes through slit A. The point-like photon counting detector  $D_2$  is located 500 mm behind “screen B.” “Screen B” is the image plane defined by the Gaussian thin equation. Slit B, either adjusted as the same size as that of slit A or opened completely, is placed to coincide with the ghost image. The output pulses from the detectors are sent to a coincidence circuit. During the measurements, the bucket detector  $D_1$  is fixed behind slit A while the point detector  $D_2$  is scanned on the  $y$ -axis by a step motor.

**Measurement 1** Measurement 1 studied the case in which both slits A and B were adjusted to be 0.16 mm. The  $y$ -coordinate of  $D_1$  was chosen to be 0 (center) while  $D_2$  was allowed to scan along its  $y$ -axis. The circled dot data points in ■ Fig. 16.24 show the *coincidence* counting rates against the  $y$ -coordinates of  $D_2$ . It is a typical single-slit diffraction pattern with  $\Delta y \Delta p_y = h$ . Nothing is special in this measurement except that we have learned the width of the diffraction pattern for the 0.16 mm slit and this represents the minimum uncertainty of  $\Delta p_y$ . We should emphasize at this point that the *single* detector counting rate of  $D_2$  as a function of its position  $y$  is basically the same as that of the coincidence counts except for a higher counting rate.

**Measurement 2** The same experimental conditions were maintained except that slit B was left wide open. This measurement is a test of Popper’s prediction. The  $y$ -coordinate of  $D_1$  was chosen to be 0 (center) while  $D_2$  was allowed to scan along its  $y$ -axis. Due to the entangled nature of the signal-idler photon pair and the use of coincidence measurement circuit, only those twins which have passed through slit A and the “ghost image” of slit A at screen B with an uncertainty of  $\Delta y = 0.16 \text{ mm}$  (which is the same width as the real slit B we have used in measurement 1) would contribute to the coincidence counts through the joint detection of  $D_1$  and  $D_2$ . The diamond dot data points in ■ Fig. 16.24 report the measured coincidence counting rates against the  $y$  coordinates of  $D_2$ . The measured width of the pattern is narrower than that of the diffraction pattern shown in measurement 1. It is also interesting to notice that the single detector counting rate of  $D_2$  keeps constant in



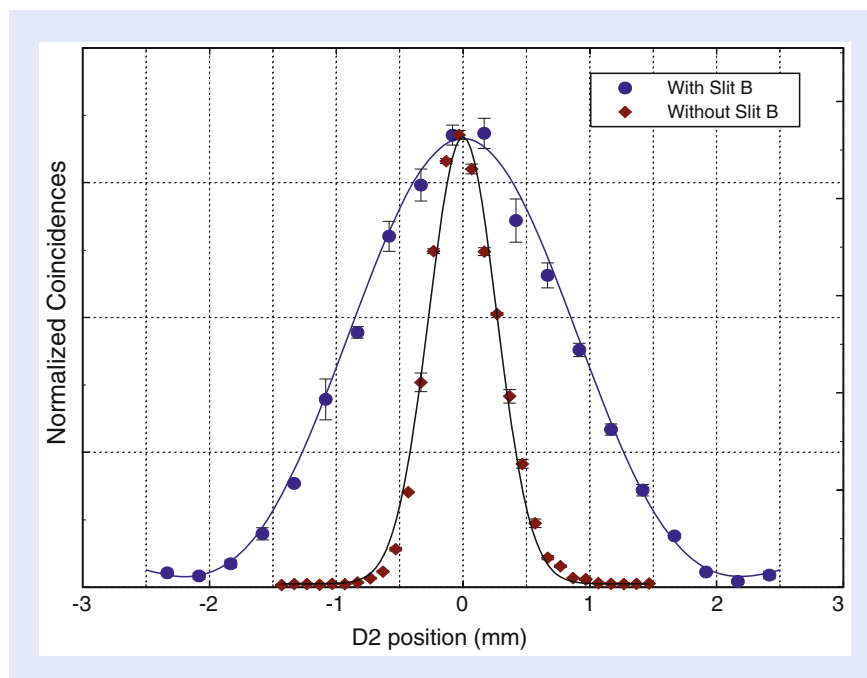


**Fig. 16.24** The observed coincidence patterns. The  $y$ -coordinate of  $D_1$  was chosen to be 0 (center) while  $D_2$  was allowed to scan along its  $y$ -axis. *Circled dot points*: Slit A = Slit B = 0.16 mm. *Diamond dot points*: Slit A = 0.16 mm, Slit B wide open. The width of the sinc-function curve fitted by the *circled dot points* is a measure of the minimum  $\Delta p_y$  determined by a 0.16 mm slit. The fitting curve for the *diamond dots* is numerical result of Eq. (16.83), indicating a *blurred ghost image* of slit A

the entire scanning range, which is very different from that in measurement 1. The experimental data has provided a clear indication of  $\Delta y \Delta p_y < h$  in the joint measurements of the entangled photon pairs.

Given that  $\Delta y \Delta p_y < h$ , is this a violation of the uncertainty principle? Does quantum mechanics agree with this peculiar experimental result? If quantum mechanics does provide a solution with  $\Delta y \Delta p_y < h$  for photon 2, we would indeed be forced to face a paradox as EPR had pointed out in 1935.

Quantum mechanics does provide a solution that agrees with the experimental result. However, it is not the solution for photon 2. Instead, it is for a joint measurement of the entangled photon pair.

We now examine the experimental results with the quantum mechanical calculation by adopting the formalisms from the ghost image experiment with two modifications:

**Case (I):** - slits A = 0.16 mm, slit B = 0.16 mm.

This is the experimental condition for measurement one: slit B is adjusted to be the same as slit A. There is nothing surprise for this measurement. The measurement simply provides us the knowledge of  $\Delta p$  of photon 2 after the diffraction caused by slit B of  $\Delta y = 0.16$  mm. The experimental data shown in **Fig. 16.24** agrees with the calculation. Notice that slit B is about 745 mm far away from the 3 mm two-photon source, the angular size of the light source is roughly the same as  $\lambda/\Delta y$ ,  $\Delta\theta \sim \lambda/\Delta y$ , where  $\lambda = 702$  nm is the wavelength and  $\Delta y = 0.16$  mm is the width of the slit. The calculated diffraction pattern is very close to that of the “far-field” Fraunhofer diffraction of a 0.16 mm single-slit.

**Case (II):** - slit A = 0.16 mm, slits B  $\sim \infty$  (wide open).

Now we remove slit B from the ghost image plane. The calculation of the transverse effective two-photon wavefunction and the second-order correlation is the same as that of the ghost image except the observation plane of  $D_2$  is moved from the image plane a distance of 500 mm behind. The two-photon image of slit A is located at a distance  $s_i = 2f = 1000$  mm ( $b_1 + b_2$ ) from the imaging lens, in this measurement  $D_2$  is placed at  $d = 1500$  mm from the imaging lens. The measured pattern is simply a “blurred” two-photon image of slit A. The “blurred” two-photon image can be calculated from Eq. (16.83)

$$\begin{aligned} \Psi(\vec{p}_o, \vec{p}_2) &\propto \int_{lens} d\vec{p}_l G\left(|\vec{p}_2 - \vec{p}_l|, \frac{\omega}{cd}\right) G\left(|\vec{p}_l|, \frac{\omega}{cf}\right) G\left(|\vec{p}_l - \vec{p}_o|, \frac{\omega}{cs_o}\right) \\ &\propto \int_{lens} d\vec{p}_l G\left(|\vec{p}_l|, \frac{\omega}{c}\left[\frac{1}{s_o} + \frac{1}{d} - \frac{1}{f}\right]\right) e^{-i\frac{\omega}{c}\left(\frac{\vec{p}_o}{s_o} + \frac{\vec{p}_l}{d}\right) \cdot \vec{p}_l} \end{aligned} \quad (16.83)$$

where  $d$  is the distance between the imaging lens and  $D_2$ . In this measurement,  $D_2$  was placed 500 mm behind the image plane, i.e.,  $d = s_i + 500$  mm. The numerical calculated “blurred” image, which is narrower than that of the diffraction pattern of the 0.16 mm slit B, agrees with the measured result of Fig. 16.24 within experimental error.

The measurement does show a result of  $\Delta y \Delta p_y < h$ . The measurement, however, has nothing to do with the uncertainty relation that governs the behavior of photon 2 (the idler). Popper and EPR were correct in the prediction of the outcomes of their experiments. Popper and EPR, on the other hand, made the same error by applying the results of two-particle physics to the explanation of the behavior of an individual particle.

In both the Popper and EPR experiments, the measurements are *joint detection* between two detectors applied to entangled states. Quantum mechanically, an entangled two-particle state only provides *the precise knowledge of the correlations of the pair*. The behavior of *photon 2* observed in the joint measurement is conditioned upon the measurement of its twin. A quantum must obey the uncertainty principle but the *conditional behavior* of a quantum in an entangled biparticle system is different in principle. We believe paradoxes are unavoidable if one insists the *conditional behavior* of a particle is the *behavior* of the particle. This is the central problem in the rationale behind both Popper and EPR.  $\Delta y \Delta p_y \geq h$  is not applicable to the conditional behavior of either *photon 1* or *photon 2* in the experiments of Popper and EPR.

The behavior of photon 2 being conditioned upon the measurement of photon 1 is well represented by the two-photon amplitudes. Each of the *straight lines* in Fig. 16.22 corresponds to a two-photon amplitude. Quantum mechanically, the superposition of these two-photon amplitudes is responsible for a “click-click” measurement of the entangled pair. A “click-click” joint measurement of the two-particle entangled state projects out certain two-particle amplitudes, and only these two-particle amplitudes are featured in the quantum formalism. In the above analysis we never consider photon 1 or photon 2 *individually*. Popper’s question about the momentum uncertainty of photon 2 is then inappropriate. The correct question to ask in these measurements should be: what is the uncertainty of  $\Delta p_y$  for the signal-idler *pair* which are localized within  $\Delta y = 0.16$  mm at “screen” A with and without slit B? This is indeed the central point for Popper’s experiment.

Once again, the demonstration of Popper's experiment calls our attention to the important message: the physics of the entangled two-particle system must inherently be very different from that of individual particles.

### 16.4.2 Popper's Experiment Two

In fact, the nonfactorizable, point-to-point image-forming correlation is not only the property of entangled photon pairs; it can also be realized in the joint-detection of a randomly paired photons in thermal state. In 2005, 10 years after the first ghost imaging experiment, a near-field lensless ghost imaging experiment that uses chaotic-thermal radiation source was demonstrated by Valencia et al. [38]. This experiment opened a door for the realization of Popper's thought experiment through the joint measurement of randomly paired photons in thermal state.

With the help of a novel joint detection scheme, namely the photon-number fluctuation correlation (PNFC) circuit [30], which distinguishes the positive and negative photon-number fluctuations measured by two single-photon counting detectors, and calculates the correlation between them, we were able to produce the ghost image of an object at a distance with 100 % visibility. By modifying the 1999 Kim-Shih experiment with a different light source and a lensless configuration, Peng and Shih realized Popper's thought experiment again in 2015 [14].

Figure 16.25 is an unfolded schematic, in which a large enough angular sized thermal source produces an equal-sized ghost image of slit-A at the plane  $d_B = d_A$ . The ghost image of slit-A can be verified by scanning the point-like photodetector  $D_B$  in the plane of slit-B. This ghost image provides the value of  $\Delta y$  through the

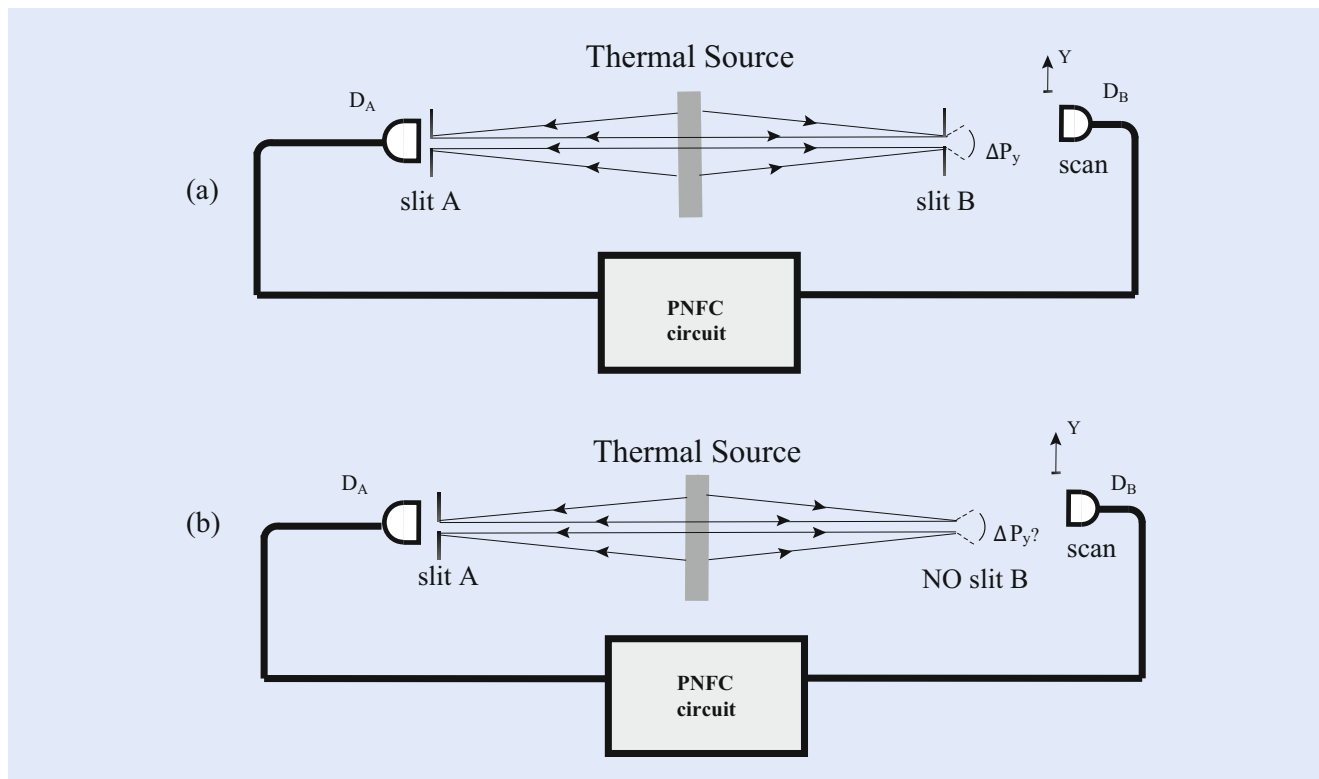
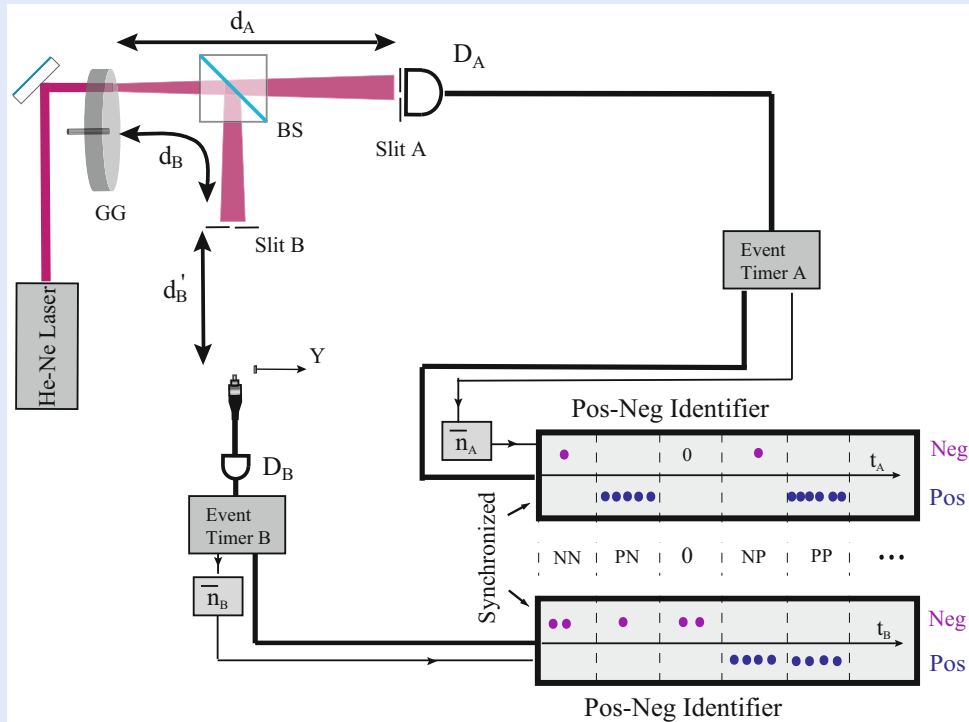


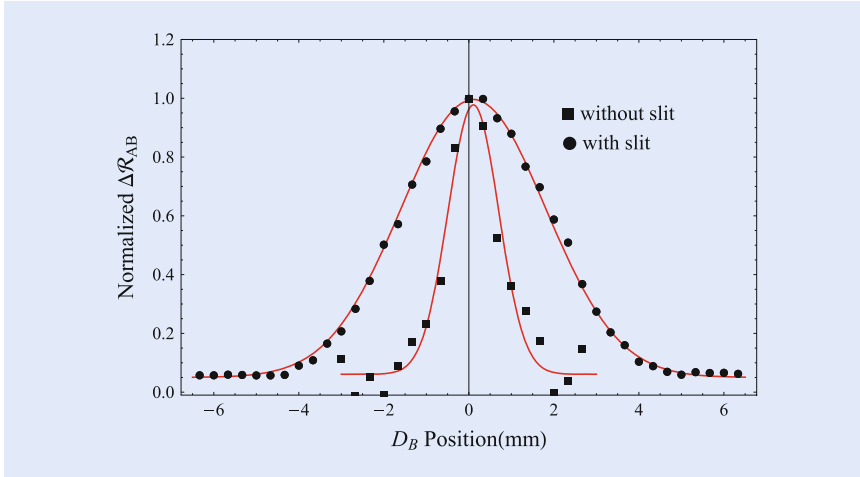
Fig. 16.25 Unfolded schematic of Popper's experiment with thermal light. The lensless ghost imaging setup with PNFC protocol produces an equal sized 100 % visibility ghost image of slit-A at the position of slit-B. Detector  $D_B$  is scanning transversely in the  $y$  direction to measure the photon-number fluctuation correlation with  $D_A$  when (a) Slit-A and slit-B are adjusted both very narrowly, and (b) Slit-A is kept very narrow and slit-B is left wide open



**Fig. 16.26** Schematic of the experimental setup. A rotating ground glass (GG) is employed to produce pseudo-thermal light. BS is a 50/50 non-polarizing beam splitter. After BS, the transmitted beam passes through slit-A (0.15 mm) and collected by a “bucket” detector  $D_A$  which is put right after the slit. The reflected beam passes slit-B, which can be adjusted to be the same width as that of slit-A or wide open, and then reaches the scanning detector  $D_B$ . The distances from slit-A and slit-B to the source are the same ( $d_A = d_B = 400$  mm). The distance from the scanning fiber tip of  $D_B$  to the plane of slit-B is  $d_B' = 900$  mm. A PNFC protocol is followed to evaluate the photon-number fluctuation correlations from the coincidences between  $D_A$  and  $D_B$

correlation measurement. Again, the question of Popper is: Do we expect to observe a diffraction pattern that satisfies  $\Delta p_y \Delta y > h$ ? To answer this question, we again make two measurements following Popper’s suggestion. Measurement-I is illustrated in the upper part of **Fig. 16.25**. In this measurement, we place slit-B, which has the same width as that of slit-A, coincident with the 1:1 ghost image of slit-A and measure the diffraction pattern by scanning  $D_B$  along the  $y$ -axis in far-field. In this measurement, we learn the value of  $\Delta p_y$  due to the diffraction of a real slit of  $\Delta y$ . Measurement-II is illustrated in the lower part of **Fig. 16.25**. Here, we open slit-B completely, scanning  $D_B$  again along the same  $y$ -axis to measure the “diffraction” pattern of the 1:1 ghost image with the same width as slit-A. By comparing the observed pattern width in measurement-II with that of measurement-I, we can examine Popper’s prediction.

The experimental details are shown in **Fig. 16.26**. The light source is a standard pseudo-thermal source, consisting of a He-Ne laser beam and a rotating ground glass (GG). A 50/50 beamsplitter (BS) is used to split the pseudo-thermal light into two beams. One of the beams illuminates a single slit, slit-A, of width  $D = 0.15$  mm located  $d_A \sim 400$  mm from the source. A “bucket” photodetector  $D_A$  is placed right behind slit-A. An equal-sized ghost image of slit-A is then observable from the positive-negative photon-number fluctuation correlation measurement between the “bucket” detector  $D_A$  and the transversely scanning point-like photodetector  $D_B$ , if  $D_B$  is scanned on the ghost image plane located at  $d_B = d_A = 400$  mm. In this experiment, however,  $D_B$  is scanned on a plane that is located  $d_B \sim 900$  mm behind the ghost image plane, to measure the “diffraction”



■ **Fig. 16.27** The observed diffraction patterns. *Circles*: slit-A and slit-B are both adjusted for 0.15 mm. *Squares*: slit-A is 0.15 mm, slit-B is wide open. The width of the curve without the slit is almost three times narrower than that of the curve with slit, agreeing well with the theoretical predictions from Eqs. (16.89) and (16.91)

pattern of the ghost image. The output pulses from the two single-photon counting detectors are then sent to a PNFC circuit, which starts from two Pos-Neg identifiers follow two event-timers distinguish the “positive-fluctuation”  $\Delta n^+$ , from the “negative-fluctuation”  $\Delta n^-$ , measured by  $D_A$  and  $D_B$ , respectively, within each coincidence time window. The photon-number fluctuation-correlations of  $D_A$ - $D_B$ :  $\Delta R_{AB} = \langle \Delta n_A \Delta n_B \rangle$  is calculated, accordingly and respectively, based on their measured positive-negative fluctuations. The detailed description of the PNFC circuit can be found in [30].

The experiment was performed in two steps after confirming the 1:1 ghost image of slit-A. In measurement-I, we place slit-B ( $D = 0.15$  mm) coincident with the ghost image and move  $D_B$  to a plane at  $d'_B \sim 900$  mm to measure the diffraction pattern of slit-B. In measurement-II, we keep the same experimental condition as that of measurement-I, except slit-B is set wide open.

■ Figure 16.27 reports the experimental results. The circles show the normalized photon-number fluctuation correlation from the PNFC protocol against the position of  $D_B$  along the y-axis for Popper’s measurement-I. As expected, we observed a typical single-slit diffraction pattern giving us the uncertainty in momentum,  $\Delta p_y^{\text{real}}$ . The squares show the experimental observation from the PNFC for Popper’s measurement-II, when slit-B is wide open. The measured curves agree well with our theoretical fittings. We found the width of the curve representing no physical slit is much narrower than that of the real diffraction pattern, which agrees with Popper’s prediction.

Similar to our early analysis in Bell state and in quantum eraser, we chose the coherent state representation for the calculation of the joint photodetection counting rate of  $D_A$  and  $D_B$  which is proportional to the second-order coherence function  $G_{AB}^{(2)}$ :

$$G_{AB}^{(2)} = \left\langle \left\langle \hat{E}^{(-)}(\vec{\rho}_A, z_A, t_A) \hat{E}^{(-)}(\vec{\rho}_B, z_B, t_B) \right. \right. \\ \left. \left. \times \hat{E}^{(+)}(\vec{\rho}_A, z_B, t_B) \hat{E}^{(+)}(\vec{\rho}_A, z_A, t_A) \right\rangle_{\text{QM}} \right\rangle_{\text{Es}}, \quad (16.84)$$

where  $E^{(+)}(\vec{\rho}_j, z_j, t_j)$  ( $E^{(-)}(\vec{\rho}_j, z_j, t_j)$ ) is the positive (negative) field operator at space-time coordinate  $(\vec{\rho}_j, z_j, t_j)$ ,  $j = A, B$ , with  $(\vec{\rho}_j, z_j, t_j)$  the transverse,

longitudinal, and time coordinates of the photodetection event of  $D_A$  or  $D_B$ . Note, in the Glauber-Scully theory [25, 36], the quantum expectation and classical ensemble average are evaluated separately, which allows us to examining the two-photon interference picture before ensemble averaging.

The field at each space-time point is the result of a superposition among a large number of subfields propagated from a large number of independent, randomly distributed and randomly radiating sub-sources of the entire chaotic-thermal source,

$$\begin{aligned}\hat{E}^{(\pm)}(\vec{\rho}_j, z_j, t_j) &= \sum_m \hat{E}^{(\pm)}(\vec{\rho}_{0m}, z_{0m}, t_{0m}) g_m(\vec{\rho}_j, z_j, t_j) \\ &\equiv \sum_m \hat{E}_m^{(\pm)}(\vec{\rho}_j, z_j, t_j),\end{aligned}\quad (16.85)$$

where  $\hat{E}^{(\pm)}(\vec{\rho}_{0m}, z_{0m}, t_{0m})$  is the  $m$ th subfield at the source coordinate  $(\vec{\rho}_{0m}, z_{0m}, t_{0m})$ , and  $g_m(\vec{\rho}_j, z_j, t_j)$  is the optical transfer function that propagates the  $m$ th subfield from coordinate  $(\vec{\rho}_{0m}, z_{0m}, t_{0m})$  to  $(\vec{\rho}_j, z_j, t_j)$ . We can write the field operators in terms of the annihilation and creation operators:

$$\hat{E}_m^{(+)}(\vec{\rho}_j, z_j, t_j) = C \int d\mathbf{k} \hat{a}_m(\mathbf{k}) g_m(\mathbf{k}; \vec{\rho}_j, z_j, t_j), \quad (16.86)$$

$C$  is a normalization constant,  $g_m(\mathbf{k}; \vec{\rho}_j, z_j, t_j)$ ,  $j = A, B$ , is the optical transfer function for mode  $\mathbf{k}$  of the  $m$ th subfield propagated from the  $m$ th sub-source to the  $j$ th detector, and  $\hat{a}_m(\mathbf{k})$  is the annihilation operator for the mode  $\mathbf{k}$  of the  $m$ th subfield.

Substituting the field operators and the state, in the multi-mode coherent representation, into Eq. (16.84), we then write  $G_{AB}^{(2)}$  in terms of the superposition of a large number of effective wavefunctions, or wavepackets:

$$\begin{aligned}G^{(2)}(\vec{\rho}_B, z_B, t_B; \vec{\rho}_B, z_B, t_B) &= \left\langle \sum_{m,n,p,q} \psi_m^*(\vec{\rho}_A, z_A, t_A) \psi_n^*(\vec{\rho}_B, z_B, t_B) \psi_p(\vec{\rho}_B, z_B, t_B) \psi_q(\vec{\rho}_A, z_A, t_A) \right\rangle_{\text{Es}} \\ &= \left\langle \sum_{m,n} |\psi_m(\vec{\rho}_A, z_A, t_A) \psi_n(\vec{\rho}_B, z_B, t_B) + \psi_n(\vec{\rho}_A, z_A, t_A) \psi_m(\vec{\rho}_B, z_B, t_B)|^2 \right\rangle_{\text{Es}} \\ &= \left\langle \sum_m |\psi_m(\vec{\rho}_A, z_A, t_A)|^2 \sum_n |\psi_n(\vec{\rho}_B, z_B, t_B)|^2 \right. \\ &\quad \left. + \sum_{m \neq n} [\psi_m^*(\vec{\rho}_A, z_A, t_A) \psi_m(\vec{\rho}_B, z_B, t_B) \psi_n(\vec{\rho}_A, z_A, t_A) \psi_n^*(\vec{\rho}_B, z_B, t_B)] \right\rangle_{\text{Es}} \\ &\equiv \langle n_A \rangle \langle n_B \rangle + \langle \Delta n_A \Delta n_B \rangle.\end{aligned}\quad (16.87)$$

with

$$\psi_s(\vec{\rho}_j, z_j, t_j) = \int d\mathbf{k} \alpha_s(\mathbf{k}) e^{i\varphi_{0s}} g_s(\mathbf{k}; \vec{\rho}_j, z_j, t_j),$$

where  $s = m, n, p, q$ ,  $j = A, B$ , and the phase factor  $e^{i\varphi_{0s}}$  represents the random initial phase of the  $m$ th subfield. In Eq. (16.87), we have completed the ensemble average in terms of the random phases of the subfields, i.e.  $\varphi_{0s}$ , and kept the nonzero terms only. Equation (16.87) indicates the second-order coherence function is the result of a sum of a large number of subinterference patterns, each

subpattern indicates an interference in which a random pair of wavepackets interfering with the pair itself. For example, the  $m$ th and the  $n$ th wave packets have two different yet indistinguishable alternative ways to produce a joint photodetection event, or a coincidence count, at different space-time coordinates: (1) the  $m$ th wavepacket is annihilated at  $D_A$  and the  $n$ th wavepacket is annihilated at  $D_B$ ; (2) the  $m$ th wavepacket is annihilated at  $D_B$  and the  $n$ th wavepacket is annihilated at  $D_A$ . In quantum mechanics, the joint detection probability of  $D_A$  and  $D_B$  is proportional to the normal square of the superposition of the above two probability amplitudes. We name this kind of superposition “nonlocal interference.” The superposition of the two amplitudes for each random pair results in an interference pattern, and the addition of these large number of interference patterns yields the nontrivial correlation of the chaotic-thermal light.

The cross interference term in Eq. (16.87) indicates the photon-number fluctuation correlation  $\langle \Delta n_A \Delta n_B \rangle$ :

$$\begin{aligned} & \langle \Delta n_A(\vec{\rho}_A, z_A, t_A) \Delta n_B(\vec{\rho}_B, z_B, t_B) \rangle_{E_S} \\ &= \left\langle \sum_{m \neq n} [\psi_m^*(\vec{\rho}_A, z_A, t_A) \psi_n(\vec{\rho}_A, z_A, t_A)] [\psi_m(\vec{\rho}_B, z_B, t_B) \psi_n^*(\vec{\rho}_B, z_B, t_B)] \right\rangle_{E_S} \quad (16.88) \\ &\simeq \left\langle \sum_m \psi_m^*(\vec{\rho}_A, z_A, t_A) \psi_m(\vec{\rho}_B, z_B, t_B) \sum_n \psi_n(\vec{\rho}_A, z_A, t_A) \psi_n^*(\vec{\rho}_B, z_B, t_B) \right\rangle_{E_S}. \end{aligned}$$

In measurement-I, the optical transfer functions that propagate the fields from the source to  $D_A$  and  $D_B$  are


$$g_m(\vec{\kappa}, \omega; \vec{\rho}_A, z_A = d_A) = \frac{-i\omega e^{i(\omega/c)z_A}}{2\pi c d_A} \int d\vec{\rho}_s f(\vec{\rho}_s) e^{i\vec{\kappa} \cdot \vec{\rho}_s} G(|\vec{\rho}_s - \vec{\rho}_o|)_{[\omega/(cd_A)]},$$

and

$$\begin{aligned} & g_n(\vec{\kappa}, \omega; \vec{\rho}_B, z_B = d_B + d'_B) \\ &= \frac{-\omega^2 e^{i(\omega/c)z_B}}{(2\pi c)^2 d_B d'_B} \int d\vec{\rho}_s \int d\vec{\rho}_i f(\vec{\rho}_s) e^{i\vec{\kappa} \cdot \vec{\rho}_s} G(|\vec{\rho}_s - \vec{\rho}_i|)_{[\omega/(cd_B)]} \\ & \quad t(\vec{\rho}_i) G(|\vec{\rho}_i - \vec{\rho}_B|)_{[\omega/(cd'_B)]}, \end{aligned}$$

where  $\vec{\rho}_s$  is defined on the output plane of the source and  $f(\vec{\rho}_s)$  denotes the aperture function of the source. We also assumed a perfect “bucket” detector  $D_A$ , which is placed at the object plane of slit-A ( $\vec{\rho}_A = \vec{\rho}_o$ ), in the following calculation.  $\vec{\rho}_i$  is defined on the ghost image plane, which coincides with the plane of slit-B, and  $\vec{\rho}_B$  is defined on the detection plane of  $D_B$ ,  $t(\vec{\rho}_i)$  is the aperture function of slit-B. The function  $G(|\alpha|)_{[\beta]}$  is the Gaussian function  $G(|\alpha|)_{[\beta]} = e^{-\frac{\beta}{2}|\alpha|^2}$ . The measured fluctuation correlation can be calculated from Eq. (16.88)

$$\Delta R_{AB} = \int d\vec{\rho}_o |t(\vec{\rho}_o)|^2 \text{sinc}^2[\omega_0 D \frac{\vec{\rho}_B}{2cd_B}] \equiv C' \times \text{sinc}^2[\omega_0 D \frac{\vec{\rho}_B}{2cd_B}], \quad (16.89)$$

where  $t(\vec{\rho}_o)$  is the aperture function of slit-A. The above calculation indicates a product between a constant  $C'$ , which is from the integral on the “bucket” detector  $D_A$ , and a first order diffraction pattern of slit-B. With our experimental setup, the width of the diffraction pattern is estimated to be  $\sim 4$  mm, which agrees well with the experimental observation, as shown in  Fig. 16.27.

In measurement-II, with slit-B wide open, the field at  $D_B$  becomes

$$g_n(\vec{k}, \omega; \vec{\rho}_B, z_B) = \frac{-i\omega e^{i(\omega/c)z_B}}{2\pi c z_B} \int d\vec{\rho}_s f(\vec{\rho}_s) e^{i\vec{k} \cdot \vec{\rho}_s} G(|\vec{\rho}_s - \vec{\rho}_B|)_{[\omega/(cz_B)]}.$$

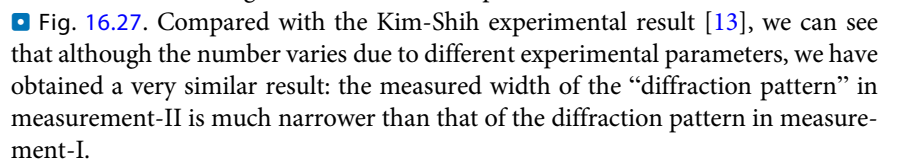
We first check if a ghost image of slit-A is present when scanning  $D_B$  in the ghost image plane of  $d_B = d_A$ . The photon-number fluctuation correlation is calculated to be

$$\begin{aligned} \Delta R_{AB} &= \int d\vec{\rho}_o |t(\vec{\rho}_o)|^2 \sin^2 c^2 \left[ \frac{\omega_0 a}{cd_A} |\vec{\rho}_o - \vec{\rho}_B| \right] \\ &= |t(\vec{\rho}_o)|^2 \otimes \sin^2 c^2 \left[ \frac{\omega_0 a}{cd_A} |\vec{\rho}_o - \vec{\rho}_B| \right] \approx |t(\vec{\rho}_B)|^2. \end{aligned} \quad (16.90)$$

Note, we have placed  $D_A$  right behind slit-A and thus  $\vec{\rho}_A = \vec{\rho}_o$ . This suggests an equal-sized 100 % visibility ghost image on the plane of  $d_B = d_A$ .

When we move  $D_B$  away from the ghost image plane to the far-field plane of  $d_B + d_{B'}$ , the photon-number fluctuation correlation becomes:

$$\Delta R_{AB} = \int d\vec{\rho}_o |t(\vec{\rho}_o)|^2 \tilde{\mathcal{F}}_s^2(m\vec{\rho}_o - \vec{\rho}_B) = |t(\vec{\rho}_o)|^2 \otimes \tilde{\mathcal{F}}_s^2(m\vec{\rho}_o - \vec{\rho}_B), \quad (16.91)$$

where  $\tilde{\mathcal{F}}_s$  is the Fourier transform of the defocused pupil function  $\mathcal{F}_s = f(\vec{\rho}_s) e^{-i(\omega_0/2c\mu)\vec{\rho}_s^2}$  and  $\mu, m$  are defined as  $1/\mu = 1/d_A - 1/(d_B + d_{B'})$ ,  $m = (d_B + d_{B'})/d_A$ , respectively. The measured result of measurement-II is thus a convolution between the aperture function of slit-A,  $t(\vec{\rho}_o)$ , and the correlation function  $\tilde{\mathcal{F}}_s(m\vec{\rho}_o - \vec{\rho}_B)$ , resulting in a “blurred” image of slit-A. With our experimental setup, the width of the “diffraction” pattern is estimated to be  $\sim 1.4$  mm, which is almost three times narrower than the diffraction pattern of measurement-I and agrees well with the experimental observation, as shown in  Fig. 16.27. Compared with the Kim-Shih experimental result [13], we can see that although the number varies due to different experimental parameters, we have obtained a very similar result: the measured width of the “diffraction pattern” in measurement-II is much narrower than that of the diffraction pattern in measurement-I.

The above analysis indicates that the experimental observations are reasonable from the viewpoint of the coherence theory of light. The important physics we need to understand is to distinguish the first-order coherent effect and the second-order coherent effect, even if the measurement is for thermal light. In Popper’s measurement-I, the fluctuation correlation is the result of first-order coherence. The joint measurement can be “factorized” into a product of two first-order diffraction patterns. After the integral of the “bucket” detector, which turns the diffraction pattern of slit-A into a constant, the joint measurement between  $D_A$  and  $D_B$  is a product between a constant and the standard first-order diffraction pattern of slit-B. There is no question the measured width of the diffraction pattern satisfies  $\Delta p_y \Delta y \geq h$ . In Popper’s measurement-II when slit-B is wide open or removed, the measurement can no longer be written as a product of single-photon detections but as a non-separable function, i.e., a convolution between the object aperture function and the photon-number fluctuation correlation function of randomly paired photons, or the second-order coherence function of the thermal field. We thus consider the observation of  $\Delta p_y \Delta y < h$  the result of the second-order coherence of thermal field which is caused from nonlocal interference: a randomly paired photon interferes with the pair itself at a distance by means of a joint photodetection event between  $D_A$  and  $D_B$ . The result of nonlocal two-photon interference does not contradict the uncertainty principle that governs the



behavior of single photons. Again, the observation of this experiment is not a violation of the uncertainty principle. The observation of  $\Delta p_y \Delta y < h$  from thermal light, however, may reveal a concern about nonlocal interference.

## 16.5 Conclusion

---

This chapter reviewed three types of optical tests of the foundations of quantum theory: (1) EPR-Bohm-Bell correlation and Bell's inequality; (2) Scully's quantum eraser; (3) Popper's experiment. The results of these experiments are very interesting. On one hand, the experimental observations confirm the predictions of EPR-Bell, Scully, and Popper. On the other hand, the calculations from quantum theory perfectly agree with the experimental data. Moreover, apparently, the experimental observations do not lead to any "violations" of the principles of quantum mechanics. One important conclusion we may draw from these optical tests is that all the observations are the results of multi-photon interference: a group of photons interferes with the group itself at distance. The nonlocal multi-photon interference phenomena may never be understood in classical theory, however, it is legitimate in quantum mechanics. The superposition principle of quantum theory supports the superposition of multi-photon amplitudes, whether the photons are entangled or randomly grouped and despite the distances between these individual photodetection events. Perhaps we must accept the probabilistic nature of the "wavefunction" associated with a quantum or a group of quanta. Although a photon does not have a "wavefunction," we have developed the concept of an effective wavefunction for a photon and for a group of photons which have similar physical meanings as that of the wavefunction of a particle or the wavefunction of a group of particles. In terms of the superposition, although the effective wavefunction plays the same role as that of the electromagnetic wave, apparently, the effective wavefunction is different from the electromagnetic field in nature. Any efforts attempting to physically equal the two concepts would trap us in the question posed by Einstein: how long does it take for the energy on the other side of the 2-lightyear diameter sphere to arrive at the detector? Is it possible god of the quantum world does play dice?

**Open Access** This chapter is distributed under the terms of the Creative Commons Attribution 4.0 International License (<http://creativecommons.org/licenses/by/4.0/>), which permits use, duplication, adaptation, distribution and reproduction in any medium or format, as long as you give appropriate credit to the original author(s) and the source, a link is provided to the Creative Commons license and any changes made are indicated.

The images or other third party material in this chapter are included in the work's Creative Commons license, unless indicated otherwise in the credit line; if such material is not included in the work's Creative Commons license and the respective action is not permitted by statutory regulation, users will need to obtain permission from the license holder to duplicate, adapt or reproduce the material.



## References

---

1. Wheeler JA (1982) A delayed choice experiment. Maryland lectures collection
2. Einstein A, Podolsky B, Rosen N (1935) Can quantum-mechanical description of physical reality be considered complete? *Phys Rev* 47:777
3. Bohm D (1951) *Quantum theory*. Prentice-Hall, New York
4. Shih YH (2011) *An introduction to quantum optics: photon and biphoton physics*. CRC press, Taylor & Francis, London

5. Feynman RF, Leighton RB, Sands ML (1965) Lectures on physics. Addison-Wesley, Reading
6. Bohr N (1928) Das Quantenpostulat und die neuere Entwicklung der Atomistik. *Naturwissenschaften* 16:245
7. Dirac P (1930) The principle of quantum mechanics. Oxford University Press, Oxford
8. Wheeler JA, Zurek WH (1983) Quantum theory and measurement. Princeton University Press, Princeton
9. Scully MO, Druhl H (1982) Quantum eraser: a proposed photon correlation Experiment concerning observation and “delayed choice” in quantum mechanics. *Phys Rev A* 25:2208
10. Kim YH, Yu SP, Kulik SP, Shih YH, Scully MO (2000) A delayed “choice” quantum eraser. *Phys Rev Lett* 84:1
11. Peng T, Chen H, Shih YH, Scully MO (2014) Delayed-choice quantum eraser with thermal light. *Phys Rev Lett* 112:180401
12. Popper K (1934) Zur Kritik der Ungenauigkeitsrelationen. *Naturwissenschaften* 22:807
13. Kim YH, Shih YH (1999) Experimental realization of Popper’s experiment: violation of the uncertainty principle? *Found Phys* 29:1849
14. Peng T, Simon J, Chen H, French R, Shih YH (2015) Popper’s experiment with randomly paired photons in thermal state. *Euro Phys Lett* 109:14003
15. Clauser JF, Shimony A (1978) Bell’s theorem. Experimental tests and implications. *Rep Prog Phys* 41:1881. An excellent review on Bell measurement before the introduction of SPDC
16. Freedman SJ, Clauser JF (1972) Experimental test of local hidden-variable theories. *Phys Rev Lett* 28:938
17. Clauser JF (1976) Experimental investigation of a polarization correlation anomaly. *Phys Rev Lett* 36:1223
18. Fry ES, Thompson PC (1976) Experimental test of local hidden-variable theories. *Phys Rev Lett* 37:465
19. Aspect A, Grangier P, Roger G (1981) Experimental tests of realistic local theories via Bell’s theorem. *Phys Rev Lett* 47:460
20. Aspect A, Grangier P, Roger G (1982) Experimental realization of Einstein-Podolsky-Rosen-Bohm gedankenexperiment: a new violation of Bell’s inequalities. *Phys Rev Lett* 49:91
21. Alley CO, Shih YH (1986) In: Namiki M et al (ed) Foundations of quantum mechanics in the light of new technology. Physical Society of Japan, Tokyo; Shih YH, Alley CO (1988) New type of Einstein-Podolsky-Rosen-Bohm experiment using pairs of light quanta produced by optical parametric down conversion. *Phys Rev Lett* 61:2921
22. Kwiat PG, Mattle K, Weinfurter H, Zeilinger A, Sergienko AV, Shih YH (1995) New high-intensity source of polarization-entangled photon pairs. *Phys Rev Lett* 75:4337
23. Klyshko DN (1988) Photons and nonlinear optics. Gordon and Breach, New York
24. Rubin MH, Klyshko DN, Shih YH, Sergienko AV (1994) The theory of two-photon entanglement in type-II optical parametric down conversion. *Phys Rev A* 50:5122
25. Glauber RJ (1963) The quantum theory of optical coherence. *Phys Rev* 130:2529
26. Kim YH, Berardi V, Chekhova MV, Shih YH (2001) Anti-correlation effect in femtosecond-pulsed type-II spontaneous parametric down-conversion. *Phys Rev A* 64:R011801
27. Kim YH, Kulk SP, Shih YH (2001) Bell state preparation using pulsed non-degenerate two-photon entanglement. *Phys Rev A* 63:R060301
28. Peng T, Shih YH (2015) Bell correlation of thermal fields in photon-number fluctuations. *Europhys Lett* 112: 60006
29. Martienssen W, Spiller E (1964) Coherence and fluctuations in light beams. *Am J Phys* 32:919
30. Chen H, Peng T, Shih YH (2013) 100% correlation of chaotic thermal light. *Phys Rev A* 88:023808
31. Glauber RJ (1963) Coherent and incoherent states of the radiation field. *Phys Rev* 131:2766
32. Bell JS (1964) On the Einstein Podolsky Rosen paradox. *Physics* 1:195
33. Bell JS (1987) Speakable and unspeakable in quantum mechanics. Cambridge University Press, Cambridge
34. Herzog TJ, Kwiat PG, Weinfurter H, Zeilinger A (1995) Complementarity and the quantum eraser. *Phys Rev Lett* 75:3034
35. Walborn SP, Terra Cunha MO, Padua S, Monken CH (2002) Double-slit quantum erasure. *Phys Rev A* 65:033818
36. Scully MO, Zubairy MS (1997) Quantum optics. Cambridge University Press, Cambridge
37. Pittman TB, Shih YH, Strekalov DV, Sergienko AV (1995) Optical imaging by means of two-photon entanglement. *Phys Rev A* 52:R3429
38. Valencia A, Scarcellì G, D’Angelo M, Shih YH (2005) Two-photon imaging with thermal light. *Phys Rev Lett* 94:063601